Electron microscopy at atomic resolution

B. K. Vaĭnshteĭn

A. V. Shubnikov Institute of Crystallography, Academy of Sciences of the USSR, Moscow
Usp. Fiz. Nauk **152**, 75–122 (May 1987)

Contemporary transmission electron microscopes have resolutions down to 1.5–2 Å, and this enables one to observe atoms directly. A theory is presented of the formation of electron-microscope images at atomic resolution, the influence of aberrations, the properties of the transfer function, and the methods of processing, calculating, and interpreting images. The relation is examined between electron microscopy and electron diffraction. Examples are given of electron-microscope studies of the atomic structure of various objects—molecules, crystals, various organic and inorganic compounds, including minerals and semiconductors, and of studies of defects of crystal-structure and of its formation during crystal growth.

TABLE OF CONTENTS

1. INTRODUCTION

Electron microscopy has already existed for more than half a century—in 1932 Knoll and Ruska built the first two-lens electron microscope.[1,2] A long-standing dream of electron microscopists—to obtain a direct image of atoms in molecules or crystals—has now already been achieved, and EM[1] at atomic resolution has become a working instrument of physicists, crystallographers, chemists, and materials scientists. This dream has rested on the understanding that the short wavelength of electrons allows one in principle to resolve atoms:

$$\lambda = h\,(2meV^*)^{-1/2} \approx 12.26\,V^{*-1/2} \qquad (1)$$

(here λ is in Å, where 1 Å = 0.1 nm, and V^* is the accelerating potential V in volts with the relativistic correction $V^* = V\,[1 + (eV/2mc^2)]$.) Thus, when $V = 100$ kV, $\lambda = 0.037$ Å; the Rayleigh criterion for resolution of a microscope with an angular aperture α_0—the radius of the "disk of confusion"—is

$$\delta_D = 0.61\lambda\alpha_0^{-1}. \qquad (2)$$

The distance between atoms lies in the range 1–4 Å, and it would seem that one could easily resolve atoms by choosing an appropriate α_0. However, in practice the resolution is not determined by the diffraction criterion (2), but by the aberrations of the magnetic lenses of the em system, and mainly by the spherical aberration C_s of the objective lens. Here the disk of confusion has the radius $\delta_s \approx 1/4C_s\alpha_0^3$. Thus, if we increase the aperture α_0, as is favorable from the standpoint of the diffraction criterion (2), we lose in cubic fashion owing to spherical aberration. The optimal α_0 is determined by the transfer function T of the objective lens with account taken of the defocus, and the actual resolution is

$$\delta = \frac{\lambda}{\alpha_0} \approx 0.6\,\lambda^{3/4}C_s^{1/4}. \qquad (3)$$

The magnitude of C_s of the best modern electron microscopes at 100 kV amounts to 1–0.7 mm, which yields $\delta \approx 2$ Å. This already actually allows one to resolve atoms, although one would wish to obtain even a higher resolution. The pathway to doing this is to improve the design of the instruments as a whole and to improve the lenses (but C_s enters into (3) only to the 1/4 power—a very weak dependence), to impose special requirements on the specimens, and principally, to increase the accelerating potential. Thus, for $V = 1$ MV we have $\lambda = 0.009$, and the resolution is $\delta \approx 1$ Å. However, an increase in the potential entails a considerable complication in the design of the microscope. The optimal results are obtained now in commercial highly perfected instruments with an accelerating potential of 100–300 kV and in specialized microscopes with potentials 400 kV–1 MV (there are even instruments with a potential of 3 MV). In essence the entire postwar history of the experimental transmission electron

 0038-5670/87/050393-27$01.80

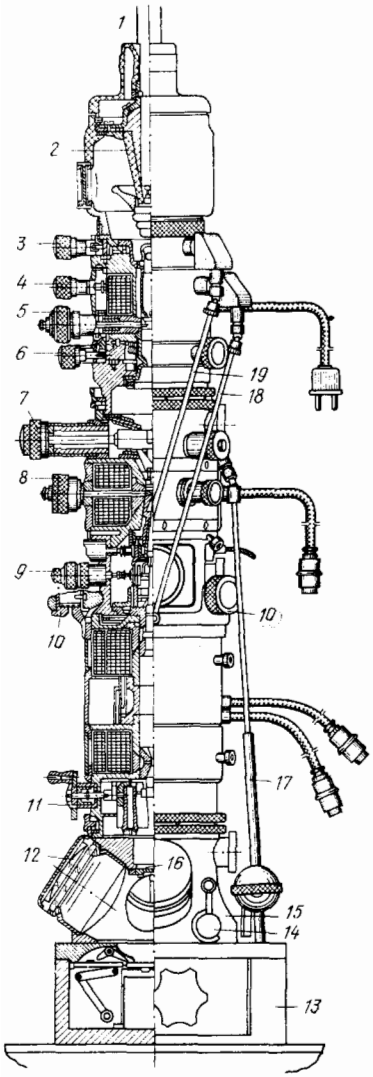

FIG. 1. Diagram of the column of a modern transmission electron microscope. 1—high-voltage cable, 2—insulator, 3—mechanism for aligning the gun, 4—mechanism for tilting the illumination system, 5—knob for aligning and changing the condenser diaphragm, 6—knob for plane-parallel translation of the condenser, 7—specimen airlock, 8—knob for aligning the objective diaphragm, 9—knob for interchangeable microdiffraction diaphragms, 10—knob for aligning the objective, 11—knob for removing the pole piece of the projection lens, 12—window for observing the image, 13—photocamera, 14—knob of the photocamera airlock, 15—housing of the projection lens, 16—cover of the photocamera airlock, 17—rod for translating the specimen, 18—rod for aligning the illumination system, 19—rod for aligning the gun.

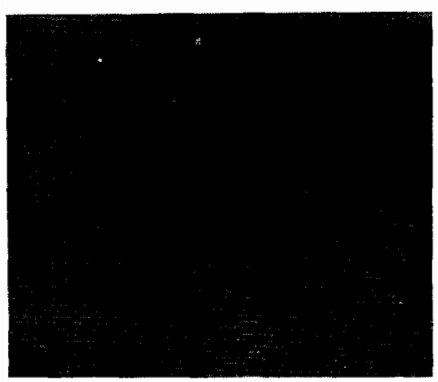

FIG. 2. One of the first electron micrographs of planes of a crystal lattice (phthalocyanine) taken by Menter in 1956.[3] Distance between planes ~12 Å.

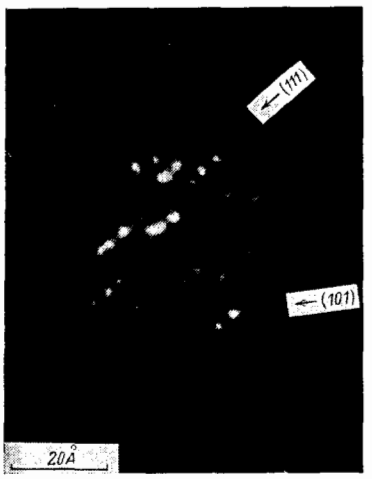

FIG. 3. Dark-field electron micrograph of a microcrystal of ThO_2.[4] Bright spots are thorium atoms.

microscope has been one of competition of different groups of scientists and engineers who have created ever more refined models of microscopes, at which the Japanese, West German, and Dutch instrument builders have excelled more than others.

The contemporary transmission electron microscope is one of the most complicated physical instruments (Fig. 1). The construction of its parts, especially the parts of the optical system, uses special materials and requires extreme accuracy. The column of the instrument must be very vibration-stable, and special foundations and suspension systems are created for high-voltage instruments. A great stability of the accelerating potential ($\sim 10^{-6}$) and of the lens-supply current is required. The direct electron-optic magnification is as much as 60 000–1 300 000. The photographs are usually further enlarged photographically by a factor of 5–20.

In the small space inside the objective ($\varnothing \sim 2$ mm), miniature specimen holders are introduced having a goniometric head that enables orienting crystalline specimens as needed. The microscopes are supplied with attachments for operating in a cooling or heating mode, for scanning, for x-ray microanalysis, etc. The visualization of the image on the

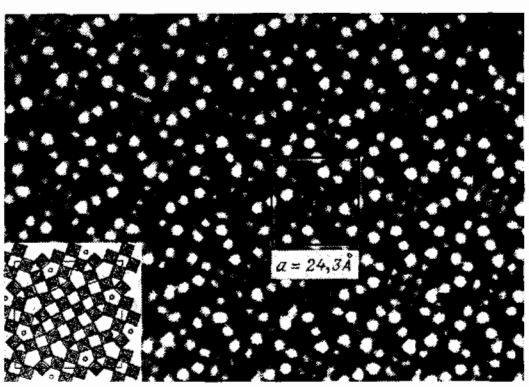

FIG. 4. One of the numerous examples of em observation of a crystal structure—a projection of the tetragonal crystal $2Nb_2O_5 \cdot 7WO_3$.[5] In the inset at lower left the quadrilaterals are projections of MeO_6 octahedra. In the electron micrograph: dark sites—metal atoms, bright sites—empty vertical channels in the structure; JEM 100 B microscope, accelerating potential 100 kV.

screen (and subsequently photographically) is supplemented by other recording devices with output of the em pattern on a display.

In 1956 Menter obtained the first images of "planes" of a crystal lattice (Fig. 2),[3] and later a number of authors obtained images of atoms and groups of atoms in crystals (Fig. 3)[4] and of crystal structures (Fig. 4).[5] The theory of formation and calculation of em images, which is closely connected with the theory of electron diffraction[17] and methods of processing of em data,[18–20] were intensively developed in the studies of Scherzer,[6] Siegel,[7] Hoppe,[8] Cowley,[9–11] and many other authors.[12–16] The original literature on electron microscopy includes tens of thousands of authors, a number of books[1,21–28] have been published, and electron microscopists gather at international, regional, and All-Union conferences, congresses, and symposia.

2. THE ELECTRON-MICROSCOPE IMAGE

The electron beam produced by the illumination system is incident on the object and is scattered by it. The scattered wave is transformed by the objective lens into an image, which upon subsequent magnification is transferred to the screen by a system of projection lenses (Fig. 5a).

The wave function of the image ψ_i can be written as:

$$\psi_i = \tilde{\mathfrak{F}}^{-1} T \tilde{\mathfrak{F}} q \psi_0; \tag{4}$$

Here ψ_0 is the incident wave. Upon passing through the object, the wave ψ_0 interacts with its potential φ. Consequently, at the exit surface of the object the wave acquires the form $q\psi_0$, where q is the so-called transmission function. The scattering or diffraction of the wave $q\psi_0$ is described by the action of the Fourier operator $\tilde{\mathfrak{F}}$, which determines the wave function in the back focal plane of the objective lens. In turn, this function is modified by the transfer function T of the lens. The transformation of the scattered wave into the image is described by the inverse Fourier transform operator $\tilde{\mathfrak{F}}^{-1}$. Let us examine all these stages in turn.

3. SCATTERING OF ELECTRONS BY AN OBJECT. KINEMATIC APPROXIMATION

In the Schrödinger equation

$$\nabla^2\psi + 8\pi^2 m h^{-2} [eV + e\varphi(\mathbf{r})]\psi = 0 \tag{5}$$

eV is the energy of the incident wave, and $e\varphi(\mathbf{r})$ is the potential energy of an electron in the object. Thus the "scattering material" for electrons is the electrostatic potential $\varphi(\mathbf{r})$, which is formed by superposition of the potentials of the atoms of the object.[17] The potential of each of the atoms is composed of the Coulomb potential of the nucleus $+Ze/r$ and the negative potential of the electrons of the shells screening the nucleus.[2)] Let the incident plane wave $\psi_0 = \exp(-i\mathbf{k}_0\cdot\mathbf{z})$ propagate in the z direction. After passing through the object, we can represent it in the form $\psi = \psi_0 + \psi'$, where ψ' is the scattered wave. The solution has the form of a spherical wave:

$$\psi' = -\frac{1}{4\pi}\frac{8\pi^2 m}{h^2}\int e\varphi(\mathbf{r})(\psi_0 + \psi')\frac{\exp(i\mathbf{kR})}{R}\,dv_{\mathbf{r}_1} \tag{6a}$$

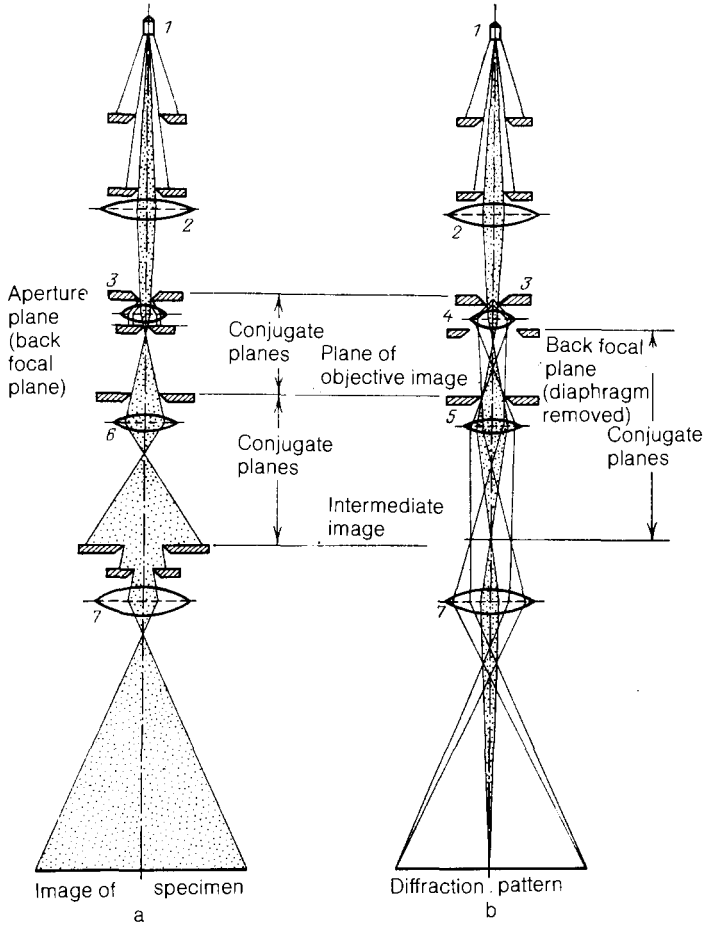

FIG. 5. Path of the rays in the transmission electron microscope. a—In an imaging mode; the image produced by the objective lens is transferred to the screen by the system of projection lenses. b—In a microdiffraction mode; the diffraction pattern is transferred to the screen; 1—source, 2—condenser lens, 3—specimen, 4—objective lens, 5—selector diaphragm, 6—intermediate lens, 7—projection lens.

($\mathbf{R} = \mathbf{r} - \mathbf{r}'$). The meaning of this expression is the following. Scattered waves arise as both the initial wave ψ_0 and the scattered waves ψ' themselves pass through the object. As the initial wave ψ_0 penetrates into the object, e.g., a crystal, the waves arising from it gradually extract its energy and themselves begin to become ever more intense. However, in the first stages—at low thicknesses—the scattered waves are weak, and correspondingly the initial wave is hardly attenuated. This is the so-called kinematic scattering. In this case one can neglect the term ψ' under the integral—the first Born approximation.[29] With increasing thickness of the object ψ' increases, while ψ_0 declines, and the scattered waves begin to interfere with the initial wave and with one another. This is the so-called dynamic scattering.[30,31]

In the kinematic approximation at a great distance from the object (Fraunhofer diffraction), the scattered wave is written as

$$\psi' = \frac{-1}{4\pi} \frac{\exp(ikR)}{R} \cdot \frac{8\pi^2 me}{h^2} \int \varphi(\mathbf{r}) \exp[i(\mathbf{k} - \mathbf{k}_0)\mathbf{r}]\, dv_{\mathbf{r}}. \tag{6b}$$

Upon introducing the vector $\mathbf{S} = (\mathbf{k} - \mathbf{k}_0)/2\pi$, we obtain the expression for the kinematic scattering amplitude as a Fourier expansion of the potential[17,29]:

$$\Phi(\mathbf{S}) = \int \varphi(\mathbf{r}) \exp(2\pi i \mathbf{S}\mathbf{r})\, dv_{\mathbf{r}} = \int \varphi(\mathbf{r}) \exp[2\pi i (xX + yY + zZ)]\, dx\, dy\, dz = \mathfrak{F}\varphi, \tag{7a}$$

This amounts to nothing other than the Fourier integral of the potential $\varphi(\mathbf{r})$. Its absolute value is

$$\Phi_{abs} = K\Phi(\mathbf{S}), \quad K = \frac{2\pi me}{h^2}. \tag{7b}$$

The vector $\mathbf{S}$ is a vector of reciprocal space (Fourier space) having the coordinates XYZ, $|\mathbf{S}| = 2\sin\theta/\lambda \approx \alpha/\lambda$, where $\alpha = 2\theta$ is the scattering angle, which is small for electrons, and θ is the half-angle (Bragg-Wulff angle) customary for crystallographers. For each $\mathbf{k}$ the vector $\mathbf{S}$ lies on a spherical surface, the Ewald sphere (Fig. 6). If the incident wave lies in the z direction, then the scattering is determined by the projection of the potential in this direction:

$$\varphi(xy) = \int \varphi(xyz)\, dz, \tag{8}$$

The corresponding scattering amplitude is

$$\mathfrak{F}\varphi(xy) = \Phi(XY0) = \int \varphi(xy) \exp[2\pi i (xX + yY)]\, dx\, dy. \tag{9a}$$

This is the plane section $Z = 0$ of the function $\Phi(XYZ)$ in reciprocal space (see Fig. 6). The function $\Phi(XY)$ of an individual atom or any aperiodic object is distributed continuously in this section. That is, scattering occurs at all angles α.

3.1. Diffraction by a crystal

If the object is periodic, then scattering of the beam can arise only according to the Bragg-Wulff condition $n\lambda = 2d\sin\theta$, where d is the interplanar spacing, i.e., when $\mathbf{S} = \mathbf{H}_{hkl}$; $\mathbf{H}$ is the reciprocal-lattice vector having the nodes hkl, $\mathbf{H} = d^{-1}$, $\mathbf{k} = \mathbf{k}_0 + 2\pi\mathbf{H}_{hkl}$. If z coincides with the edge

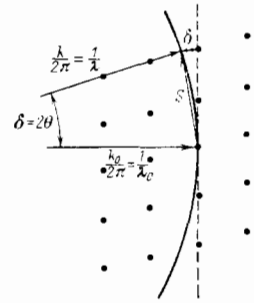

FIG. 6. The Ewald sphere in the reciprocal lattice for the case of diffraction of fast electrons ($\lambda \approx 0.05$ Å) in the region of angles in which scattering close to a plane occurs. The diffracted beams are observed for which the sphere (plane) intersects the corresponding nodes hkl of the reciprocal lattice. The dimension of the nodes is determined by the form factor of the crystal. The quantity $\delta = H^2\lambda/2$ is the deviation of the plane from the Ewald sphere.

c of the unit cell, the amplitude Φ has nonzero values at the $hk0$ nodes of the reciprocal lattice, and (9a) acquires the form

$$\Phi(XY) = \frac{1}{\Omega} \sum_{\mathbf{H}_{hk0}} \Phi_{\mathbf{H}} B(\mathbf{S} - \mathbf{H}); \tag{9b}$$

here we have also taken into account the transform $B = \mathfrak{F}b(\mathbf{r})$ of the form $b(\mathbf{r})$ of the scattering crystal that describes the form of the reciprocal-lattice nodes, and Ω is the volume of the unit cell. The condition for diffraction from the crystal is pictorially represented by the Ewald construction—one observes the beams corresponding to the intersection of reciprocal space with the sphere of reflection having the radius $k/2\pi = \lambda^{-1}$ (see Fig. 6). Owing to the smallness of λ, the corresponding region of the sphere is almost "planar," and in diffraction from crystals, especially those of small thickness, many diffracted beams can arise simultaneously.[17,32]

Thus the first stage in the formation of an EM image is the scattering of electrons by the object, or diffraction, which is described by the Fourier operator $\mathfrak{F}$ in (4). The final image is described by the inverse Fourier transform $\mathfrak{F}^{-1}$ in (4). For an ideal lens it yields the distribution of the projected potential of the object:

$$\mathfrak{F}^{-1}\Phi(XY0) = \varphi(xy) = \frac{1}{ab} \sum_{hk0} \Phi_{hk0} \exp\left[2\pi i \left(\frac{hx}{a} + \frac{ky}{b}\right)\right]. \tag{10a,b}$$

Just like the general formula (4), Eqs. (7), (10a), (11a), and (11b) describe nothing other than the optical schema of Abbe[33] of formation of an image in a microscope, but as applied to electrons (cf. Fig. 7).

The expression (10b) is written for a crystal (a and b are the periods of the unit cell of the projection). This is a Fourier series in the amplitudes Φ_{hk0}. Properly speaking, to obtain $\varphi(xy)$ experimentally is the principal problem of EM, although far from always do em images represent precisely this function.

It is best reproduced precisely under conditions of validity of the first Born approximation—at small thicknesses of the scattering object. This explains the practical importance of this approximation. In the general case—for arbitrary thicknesses, for which dynamic scattering takes

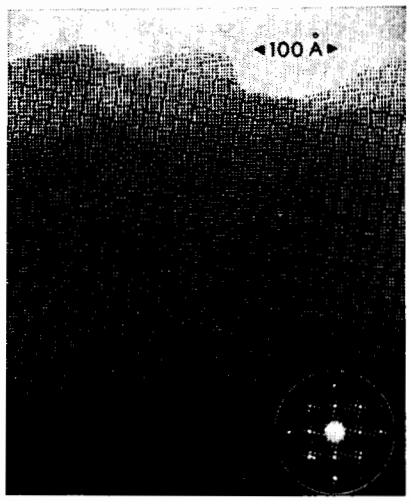

FIG. 7. Electron micrograph of the structure of the complex oxide $9Nb_2O_5 \cdot 8WO_3$ and its corresponding diffraction pattern.[34] Radius of aperture (circle) = 0.60 Å^{-1}. Resolution about 2 Å.

place—the image is also determined by the potential $\varphi(\mathbf{r})$, but all the relationships become much more complicated, and the image generally cannot be interpreted directly as the projection of the potential $\varphi(xy)$.

3.2. Transmission function

Now let us examine the form of a wave at the outer surface of an object after passing through the object having the potential $\varphi(\mathbf{r})$. If the electron scattering in the object occurs without energy loss, the action of φ gives the phase shift of the wave, or refraction. Such objects are called *phase objects*.[35-38]

The wavelength λ *in vacuo* is determined by the accelerating potential V, while λ' in the object is determined by $\varphi(\mathbf{r}) + V$. The refractive index n is

$$\frac{\lambda'^{-1}}{\lambda^{-1}} = n = \left[1 + \frac{e\varphi}{eV}\left(1 + \frac{eV}{2mc^2}\right)\right]^{1/2} \approx 1 + \frac{\varphi}{2V} \qquad (11a)$$

(φ/V is a small quantity). That is, we have

$$\frac{1}{\lambda'} = \frac{1}{\lambda} + \frac{\varphi}{2V\lambda}. \qquad (11b)$$

Thus, in the approximation that the initial wave is passing through an object of thickness A and is not scattered inside it, but accumulates phase changes, it has the following form at the exit surface:

$$q\psi_0 = \psi_0 \exp\left[2\pi i \cdot \frac{1}{2V\lambda}\int_0^A \varphi(\mathbf{r})\,dz\right] = \psi_0 \exp(i\chi). \qquad (12)$$

That is, ψ_0 acquires an extra phase shift χ determined by the projected potential $\varphi(xy)$ of (8) within the thickness of the object A:

$$\chi = -\sigma\varphi(xy), \quad \sigma = \frac{\pi}{\lambda V} = \frac{2\pi me\lambda}{h^2} = K\lambda. \qquad (13)$$

Here σ is the interaction constant [when the relativistic correction is taken into account, σ is multiplied further by $(1 + h^2m^2c^2\lambda^2)^{1/2}$].

Naturally the shift χ is maximal when the wave passes through the centers of the atoms where the value of $\varphi(\mathbf{r})$, and hence of $\varphi(xy)$, is greatest, and it is small when the wave passes between the atoms, where φ is close to zero. Yet, owing to the smallness of the interaction constant σ, the absolute magnitude of the shift is small upon passing through individual atoms or thin layers of material. If the resolution is low (not "atomic"), then we should replace the integral (8) that enters into (12) simply by $A\bar{\varphi}$, where $\bar{\varphi}$ is the mean internal potential.

Thus, on the outer surface of the object the wave ψ_0 is modified by the transmission function q of (12). Owing to the smallness of $\sigma\phi$, we can write the following[17,38] for a thin object:

$$q = \exp(i\chi) \approx 1 - i\sigma\varphi(xy) \qquad (14)$$

—the "weak-contrast" phase-object approximation. Upon assuming that the wave incident on the object has unit amplitude and zero phase at its entrance surface, we obtain $q\psi_0 = q$. As we already know, the amplitude of the wave at a great distance from the object is decribed by a two-dimensional Fourier integral—the phase function Q:

$$\mathfrak{F}q = Q(XY) \approx \delta(XY) - i\sigma\Phi(XY). \qquad (15)$$

The first terms of the expressions (14) and (15) represent the initial wave transmitted through the object in real and reciprocal spaces, while the second terms—the scattered waves that have arisen—bear information on the structure of the object. We note that, along with ψ_0, a scattered wave having the amplitude $\Phi(00)$ also propagates in the z direction.

3.3. The image. Phase and amplitude contrast

The diffraction pattern is focused in the back focal plane of the lens (see Fig. 5), and if we take XY as the coordinates in this plane, then this distribution (its amplitude and phase) amounts to the phase function $Q(XY)$. However, owing to the aberrations of the magnetic lens, this function is modified, as must be taken into account by introducing the transfer function T of the lens.[6] Consequently a distribution arises in the back focal plane that is described by the function

$$T\mathfrak{F}q = TQ(XY). \qquad (16)$$

The plane in which this function exists with its inherent amplitude-phase distribution can be treated, according to the Huygens principle, as the source of the corresponding waves. Then, according to Abbe the formation of the image having the wave function ψ_i is described in full analogy to (16) by the (inverse) Fourier transform of the function (16). That is, we arrive at the expression

$$\psi_i = \mathfrak{F}^{-1}TQ = \mathfrak{F}^{-1}T\mathfrak{F}q\ \psi_0. \qquad (4')$$

The image on the screen has the overall magnification M (created by the objective and projector lenses), the coordinates ψ_i on the screen are $x' = -Mx$, $y' = -My$, and the image is inverted. It is convenient to consider it on the scale of the object itself, and then the intensity of the image is

$$I(xy) \sim \psi_i\psi_i^*. \qquad (17)$$

The outer surface of a phase object "glows" uniformly. According to (14) the intensity on it is $|qq^*| \approx 1$, and if the action of the transfer function T in (16) did not exist, then

$\psi_i = \mathfrak{F}^{-1}q = q$, and the image (17) would also be a uniformly illuminated area.

However, as we shall see, in an optimal regime the objective lens acts so (its transfer function T is such) as to shift the phase of the scattered wave by $\pi/2$ in a certain range of scattering angles, while conserving the phase of the primary wave. Then, owing to *phase contrast*, the image reveals the projection of the potential $\varphi(xy)$. Here the mechanism is the same as in Zernike optical phase contrast, in which this contrast is attained by introducing a quarter-wave plate into the transmitted unscattered wave.[33]

Another way to obtain an image—the so-called dark-field method—is to exclude the primary wave from its formation—the term unity in (14).

Up to now we have been speaking only of elastic scattering of electrons. However, in an object, especially a thick one, inelastic scattering can also occur with loss of energy of the electrons, or they can be absorbed. In crystals these processes involve collective excitations of the electrons of the lattice (plasmons), excitation of phonons, thermal diffuse scattering, and other phenomena.[11] Altogether, one can describe these effects phenomenologically as an effective absorption $\mu(xy)$ of electrons in the object (this is, as it were, the imaginary component of the "complex" potential). The absorption also contributes to the transmission function of (14). Thus in the general case the latter has the form

$$q = \exp[-i\sigma\varphi(xy) - \mu(xy)] \approx 1 - i\sigma\varphi(xy) - \mu(xy). \tag{18}$$

Correspondingly the scattering amplitude $\mathfrak{F}_q = Q$ of (15) acquires the form

$$Q(XY) = \delta(XY) - i\sigma\Phi(XY) - M(XY). \tag{19}$$

Here $M = \mu$ describes the amplitude contrast in the image. This part would be reproduced by an ideal lens [without T in (4)] directly, but T also modifies the amplitude contrast in a definite fashion.

Thus, when certain conditions are satisfied, the em image conveys the structure of the function $\varphi(xy)$—the projection of the potential of the object, and if the instrument has sufficient resolving power, one can observe groups of atoms or individual atoms as the least "transparent" sites of the image.

3.4. Transfer function

Now let us examine the properties of the transfer function T that enters into the image-formation (4).[6,11,39] Owing to its circular symmetry it is convenient to write it as $T(U)$, where U is the radial coordinate in the XY plane of reciprocal space, i.e., in the back focal plane of the objective lens, $U = (X^2 + Y^2)^{1/2}$. The scattering angle is $\alpha = \lambda U$. The reciprocal U^{-1} corresponds to the "spatial periods" in the object, and for crystals to the interplanar spacings $d = U^{-1}$. The quantities U are the distances in reciprocal space—in electron microscopy they are often called "spatial frequencies." The function $T(U)$ consists of three components:

$$T_t(U) = D(U)\,W(U)\,G(U). \tag{20}$$

D describes the effect of the aperture diaphragm, W the action of the objective lens, and G the effect of the instabilities of the instrument.

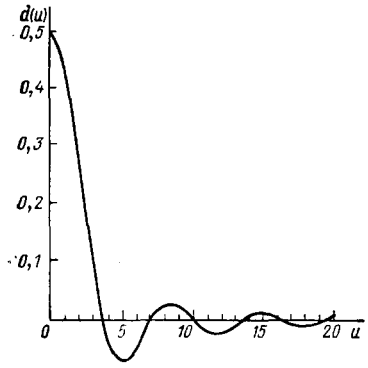

FIG. 8. Fourier-Bessel transform $d(u)$ of the aperture function of a circle of radius U_{max}.[22] The first zero of the function lies at $U = 0.61\,U_{max}^{-1}$.

In correspondence to the action of the Fourier operator $\mathfrak{F}^{-1}$ in (4), the effect of these three functions and the function $\mathfrak{F}_q = Q$ of (18) and (19) on ψ_i will be described by the convolution of the $\mathfrak{F}^{-1}$ of each of the functions:

$$\psi_i = \mathfrak{F}^{-1}D * \mathfrak{F}^{-1}W * \mathfrak{F}^{-1}G * \mathfrak{F}^{-1}Q. \tag{21}$$

The function D is the aperture, its shape, and position. For a central, circular hole with the aperture angle α_0 (see Fig. 7b), i.e., with maximum $U_{max} = \alpha_0/\lambda$, we have

$$D(U) = \begin{cases} 1 & \text{when } U \leqslant U_{max}, \\ 0 & \text{when } U > U_{max}. \end{cases} \tag{22}$$

In the image plane having the radial coordinate $u = (x^2 + y^2)^{1/2}$ we have

$$\mathfrak{F}^{-1}D = 2\pi U_{max}^2 J_1(2\pi U_{max}u)(2\pi U_{max}u)^{-1} = d(u); \tag{23}$$

here J_1 is the first-order Bessel function. The first zero of the function $d(u)$ (Fig. 8) lies at $u = 0.61\,U_{max}^{-1} = 0.61\lambda/\alpha_0$. It determines the diffraction resolving power δ_D of (2)—the "edge" of the function $d(u)$.

A very important characteristic of the electron microscope is the contrast transfer function W (CTF) of the objective lens. Depending on the coordinate U, i.e., the angle of deflection of the scattered electrons α it yields the differing phase shift $\chi_1(U)$:

$$W = \exp(i\chi_1) = \cos\chi_1 + i\sin\chi_1, \tag{24}$$

$$\chi_1 = -\frac{2\pi}{\lambda}\left(-\frac{1}{4}C_s\alpha^4 + \frac{1}{2}\Delta_f\alpha^2\right) = \frac{\pi}{2}C_s\lambda^3U^4 - \pi\lambda\Delta_fU^2; \tag{25}$$

here Δ_f is the defocus of the objective lens. Equations (24)–(25) are the famous Scherzer formula,[6] which is invariably prominent in hundreds of studies on high-resolution electron microscopy, while its CTF curve enters into the technical characterization of every microscope model. The first term of (25) is determined by the spherical aberration C_s of the objective lens, and coincides with the corresponding formula of ordinary optics. However, magnetic lenses, if compared with optical lenses, prove to be extremely imperfect, and their spherical aberration is high. This means that the outer zone of the lens deflects the electrons more strongly than the paraxial zone, and focuses them closer to the lens than the paraxial focus. The phase shift of a wave transmitted through the outer zone is larger than in the paraxial zone. However, the phase shift depends also on the defocus Δ_f of

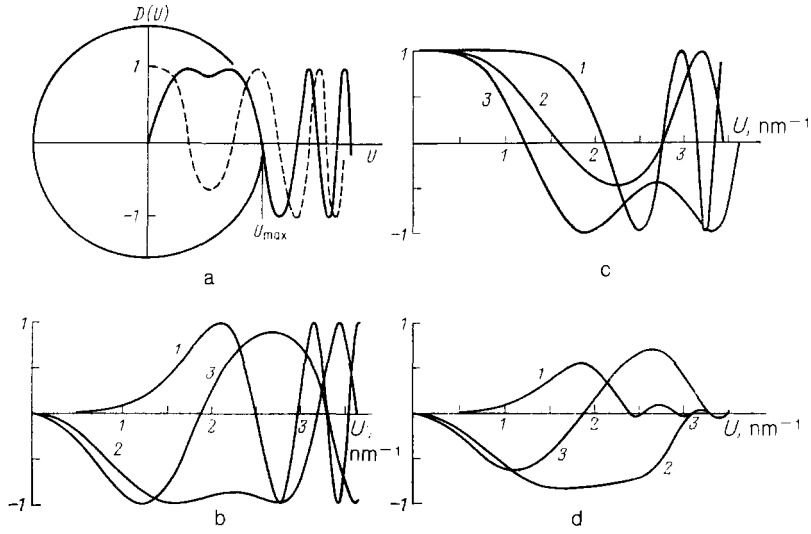

FIG. 9. a—Diagram of the contrast transfer function $W = \cos\chi_l + i\sin\chi_l$ (solid line—sin, dashed line—cos); the optimal defocus Δf_{sin} is chosen so that $\sin\chi_l$ inside the aperture (circle) does not change sign, while the oscillating part is cut off by the aperture. b—$\sin\chi_l$ and c—$\cos\chi_l$ for a 100-kV microscope, $C_s = 1.4$ mm. Curves *1*: $\Delta f = 0$, *2*: $\Delta f = -700$ Å, (optimal case); *3*: $\Delta f = -100$ Å. d—The same as Fig. 9b, but with suppression of the outer regions of the function owing to chromatic aberration. [Translator's note: Values of Δf are apparently subject to a misprint.]

the objective lens (the second term), for which, conversely, the phase shift is larger in the paraxial zone. By varying Δ_f one can attain the optimal phase shift that enables obtaining the best resolution and contrast.

Let us examine the function W. Its real and imaginary components (24) at optimal defocus are shown schematically in Fig. 9a. Both components initially vary slowly, and then begin to oscillate with a frequency of oscillations increasing with increasing U. For phase contrast, which is decisive in obtaining atomic images, the sine component of W is important. By varying the focus Δf (its magnitude and sign: " + " for underfocus, " − " for overfocus), one can obtain values of $\sin\chi_l$ close to unity in a certain interval of U, U_{max}, and when $U = 0$, $\sin\chi_l = 0$. Then, according to (4), (14)–(16), we have

$$TQ \approx Q = \delta(XY) - \sigma\Phi(XY),\ \mathfrak{F}^{-1}TQ = \psi_n \approx 1 - i\sigma\varphi(xy) = q. \qquad (26a,b)$$

Then the image intensity of (17) is the following, up to second-order terms:

$$I \sim 1 + 2\sigma\varphi(xy). \qquad (27)$$

That is, it conveys the projected potential of the object.[11]

Figure 9b shows examples of the CTF upon varying the defocus. The values $\chi_l = (\pi/2)(2n+1)$, $n = 0, \pm 1, \pm 2, \ldots$, yield the maximum contribution $\sin\chi_l = \pm 1$. Upon differentiating $d\chi/dU$ at $n = 0$, we obtain the value of Δf for optimal Scherzer defocus[21]:

$$\Delta_{Sch} = (C_s\lambda)^{1/2}. \qquad (28)$$

The first zero U_{max} of the phase-contrast function at the optimal defocus Δ_{Sch} defines the boundary of the zone of correct contrast reproduction. That is, the resolution is

$$\delta = U_{max}^{-1} \approx 0{,}7C_s^{1/4}\lambda^{3/4}. \qquad (29)$$

Naturally there is no sense in taking an aperture larger than U_{max} (see Fig. 7.8). It is true that also in the more distant alternating regions of the same sign of the oscillating function $\sin\chi_l$, the condition for correct contrast reproduction is fulfilled. However, one can use it only in certain special cases in studying crystals, when one can choose the structure of the CTF in such a way that the positions of the principal and more distant maxima coincide with the positions of the nearest and certain distant diffracted beams[39,40] (Fig. 10). Only the necessary regions of the CTF are also used in the "zone plate" method,[41] in which the alternating unneeded zones of the CTF having the opposite phase are screened.

In other estimates of the resolution, e.g., if we assume the value $\chi = 2\pi/3$ at the point of the extremum $\chi_l'(U_0)$,[11] this gives a value of the numerical coefficient in (29) of 0.66; sometimes a value about 0.5 is given.[21] The generally accepted mean value 0.6 is given in Eq. (3).

We note that an optimal value of the defocus Δf is attained not only at $n = 0$, but also at integral n in $\Delta f = [(2n+1)C_s\lambda]^{1/2}$. With an optimal choice of defocus, the image of the object is obtained in a bright-field electron micrograph in such a way that fewer electrons are incident in the images of atoms (or aggregates of them) than in the background, and they appear as dark spots (sites), while the space between them appears as bright sites. This is the so-called direct contrast. However, by varying Δf so as to shift the phase by π, we obtain contrast inversion—the dark and bright sites of the image change places. In intermediate cases the direct and inverted contrasts are superposed, and the

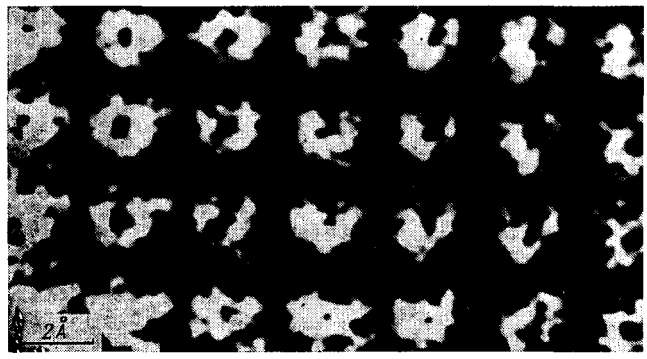

FIG. 10. In its time, this micrograph of the structure of gold (Hashimoto *et al.*[40]) appeared in many of the journals of the world. However, the "holes" at the centers of the projections of the atoms are an artifact caused by the action of the outer regions of the contrast transfer function having alternating signs.

image is not at all perceived as a certain structure. At certain defocuses (and sometimes at the optimal ones), the atoms appear to be surrounded by "halos" or they have gaps of image intensity at their centers). Of course, this does not reflect the true distribution of scattering matter in them, but represents an instrumental-diffraction effect[42,43] (Fig. 10; see below, Fig. 21).

The third factor $G(U)$ entering into (20) itself consists of three factors:

$$G(U) = g_1(\delta z)\, g_2(\delta x)\, g_3(\delta\alpha). \tag{30}$$

The most important of them is the first, which depends on the instabilities of the accelerating potential V (i.e., the nonmonochromaticity of the initial wave) and the instability of the objective lens current J and the electric fluctuations of the cathode emission δE, which have same effect:

$$\delta z = C_c\left[\left(\frac{\delta V^*}{V^*}\right)^2 + 4\left(\frac{\Delta J}{J}\right)^2 + \left(\frac{\delta E}{E}\right)^2\right]^{1/2}; \tag{31}$$

here C_c is the chromatic-aberration constant, whose magnitude is 1.2–3 mm in modern instruments. The fluctuations of the voltage and lens current are of the order of 10^{-6}, while g_2 takes account of mechanical instabilities, and g_3 takes account of the convergence of the incident electron beam, or the loss of spatial coherence. As a whole, the G of (30) displaces and blurs the outer regions of spatial frequencies responsible for the highest harmonics of the resolution, and thus suppresses them. This is expressed in the fact that the envelope $G(U)$, which declines with increasing U, is superposed on the $W(U)$ of (24) (see Fig. 9c).[44] Naturally one tries to stabilize the instrument electrically and mechanically and decrease the constant C_c so that the decline in the envelope does not affect the decisive region of W to the value of the Scherzer limit U_{max}. As a result we can form the blurring function of the image

$$\mathfrak{F}^{-1}T(U) = t(u) \approx d(u). \tag{32}$$

Here T consists of the three factors of (20)—their action is shown in Figs. 8 and 9, while $t(u)$ consists of the corresponding three components of the convolutions of (21). We must stress that the form of $t(u)$ is actually determined by the transform of the aperture $d(u)$ of (23) (see Fig. 8, and also below, Fig. 17), since the constant function $D(U)$ cuts off the function W at U_{max}, while W in turn is only blurred at large U by the function G. Yet the decisive role of the function W is determined by the phase change introduced by it in the reciprocal space U, which leads to the phase contrast of the potential, while its effect in the resultant blurring function (32) is small.

3.5. The bright-field (bf) image

This is the normal image in TEM, which, according to (18), (19), and (22), is formed from all the beams entering the aperture. It consists of a bright field from the primary beam and the image proper of the object arising from phase and amplitude contrast (Fig. 11). Upon allowing for the fact that, for a weak phase object with small absorption, q and Q are described by Eqs. (18) and (19), we can now write the following expression instead of the estimating relationships (26a,b):

$$Q' = [\delta(XY) - i\sigma\Phi(XY) - M(XY)]\exp(i\chi_1). \tag{33}$$

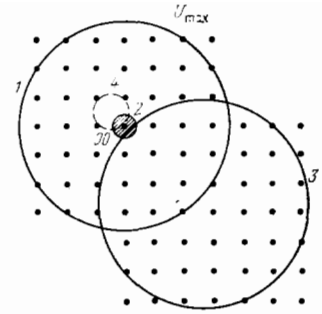

FIG. 11. The bright-field (bf) image is formed by all beams entering the aperture (circle of radius U_{max}), including the primary beam 00 (*1*); the dark-field (df) image can be obtained by blocking the primary beam 00 with a microscreen (hatched region near 00) (*2*) or by shifting the aperture (*3*), whereby the image is formed from the "side" beams; an aperture (*4*) placed "between" the reciprocal-lattice nodes will yield an image of the aperiodic components of the structure.

We obtain the following expression for ψ_i, keeping (32) in mind and neglecting G:

$$\psi_i = (1 - i\sigma\varphi - \mu) * \mathfrak{F}^{-1}\exp i\chi_1 * d(u). \tag{34}$$

The intensity of the image $I = \psi_i\psi_i^*$ is written in the following form, up to terms of second order:

$$I_{bf} \approx 1 + (2\sigma\varphi * \mathfrak{F}\ \sin\chi - \mu * \mathfrak{F}^{-1}\ \cos\chi) * d(u). \tag{35}$$

We see that the sine component of T acts on the potential, and the cosine term on the absorption, or "imaginary" potential. With an optimal choice of the aperture U_{max} at the Scherzer limit, the values of $\sin\chi_1$ at nonzero scattering angles are close to unity. Upon including them in the blur function of (32), we obtain as a result

$$I_{bf}(xy) = 1 + d(u) * [2\sigma\varphi(xy) - \mu(xy)]. \tag{36}$$

Usually the role of the term μ is small in comparison with the term $2\sigma\varphi$. For thick crystals the weak-phase-object approximation of (33) and (34) is invalid, and the calculation is performed by other methods (see below).

Since the potential $\varphi(\mathbf{r})$ in (8) has the dimensions $M^{1/2}L^{1/2}T^{-1}$, the projected potential $\varphi(xy)$ of (8) and (10a,b) revealed on electron micrographs has the dimensions $M^{1/2}L^{3/2}T^{-1}$, which formally coincides with the dimensions of charge. One can quantitatively express $\varphi(xy)$ in units of $V\cdot$Å (formally, $1\ V\cdot Å = 14.4e$). We must note that the interaction constant σ has the dimensions $M^{-1/2}L^{-3/2}T$ reciprocal to the projected potential. Hence the wave function ψ_i and also the intensity I of (35) and (36) are naturally obtained as dimensionless. For 100 kV we have $\sigma \approx 0.009$. Sometimes one assumes that in special, rarely attainable conditions (special defocus, not very thin specimen), one can describe the intensity of the image as $I \sim 1 + \lambda\Delta f\cdot\varphi''(xy)$[11,45]—this contains the second derivative of the potential, which formally has the dimensions of charge density. As we shall see below, in the dark-field method of (37) the intensity is $I \sim \varphi^2$. We must emphasize that all these functions—φ, φ^2 (and also φ'')—follow quantitatively the same course, as they have a maximum at the center of the atom and rapidly decline. Yet in practice the form of the observed spot representing an atom [see below, (46)] is that of the blurring function $d(u)$. Thus, in experimental elec-

tron microscopy in the overwhelming majority of cases, one is restricted to fixing the positions of "atom-spots" or groups of atoms and one approximately analyzes and models on a computer only the dependence of the intensity on the atomic number, which we shall take up below. Thus the main thing yielded by HREM is the geometry of arrangement of atoms in the object (in projection), and information on inclusion of foreign atoms and other defects. This renders it a powerful, pictorial method for studying the atomic-molecular structure of matter and its defects.

One can obtain exact information on the potential of atoms in diffraction structural analysis,[17] whose potentialities and limitations we shall briefly discuss below.

3.6. The dark-field (df) image

According to the scheme of Fig. 5a, the image of an object can be formed not only from electrons passing near the optical axis of the microscope with the aid of a diaphragm lying in the back focal plane, but also from any selected beams, deflected, and in particular, diffracted by a crystal. This is the so-called dark-field method, which enables one to increase the contrast and obtain additional information about the object.[47] The fundamental idea of the df method is to block with a small screen the powerful primary beam (see Fig. 11b), which in the ordinary bf method yields a strong, constant contribution to the image intensity [the terms 1 and $\delta(xy)$ in (14), (15), and (26)] on whose background the image of the structure is now revealed. In this case the optimal choice of the defocus Δf is now that at which $\cos\chi_1 \approx 1$, and $\sin\chi_1 \approx 0$. Also bearing in mind (26a,b) and (34), we obtain the following expression for the df image of a weak phase object:

$$I_{df}(xy) = \sigma^2 d^2(u) * [\varphi(xy) - \bar{\varphi}]^2. \qquad (37)$$

In contrast to the bf image, here the intensity is proportional to the square, rather than the first power of the potential. Along with the primary beam, we exclude from the image formation the scattered wave $\Phi(0)$ proceeding in the same direction [cf. (9a)], which determines the mean internal potential φ. However, the magnitude of $\bar{\varphi}$ is small in comparison with the potential of the atoms, and hence $\bar{\varphi}$ has no real value in (37).

The atoms or other, larger inhomogeneities of structure seem to "glow" in the df image, whose "background" is dark, as the primary wave is absent (Fig. 12), whereas in the bf image the atoms appear as "shadows" on the bright field. Of course, the contrast in the two cases depends also on the concrete phase relationships of the waves scattered by the object and on the transfer function, which we can vary by changing the focus. It is technically complicated to stop the central beam with a microscreen, and hence the df method is often realized in a different form—by displacing the aperture away from the central beam (see Fig. 11c), or by realizing the same idea by deflecting the primary beam (mechanically by inclining the gun or with a magnetic field) from the optical axis of the instrument outside the undisplaced aperture, into which now only the diffracted beams enter. But the set of these beams is asymmetric, and the image quality suffers.

In individual cases for revealing gross defects in crystals (not at the level of atomic resolution), e.g., dislocations, it is expedient to form the image only from an angular range of the scattered electrons near one reciprocal-lattice node—this is the so-called weak-beam method. In the case of crystals one can block the diffracted beams that bear information on the periodic component of the structure, and form the image from the electrons scattered between the reciprocal-lattice nodes (see Fig. 11d). This yields an image of the aperiodic defects, e.g., implanted atoms (Fig. 13)[48] or vacancies.

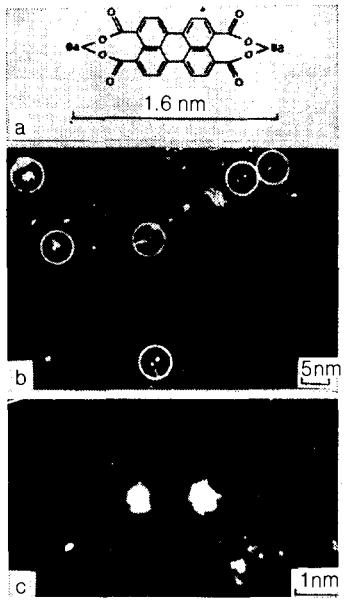

FIG. 12. A df image of Ba atoms.[46] a—Diagram of the molecule, in which the Ba atoms lie at a distance of 1.6 nm. b—A df TEM micrograph; c—The pair of Ba atoms from the circle indicated by the arrow in Fig. 12b. Ultrahigh-voltage microscope (Toulouse), accelerating potential $V = 3$ MV.

3.7. Microdiffraction

The diffraction pattern of the object is formed in the electron microscope in the back focal plane of the objective lens, and actually exists (see Figs. 5b and 7b). The square of the modulus of the second term Q of (15) or (9a), (9b) gives the intensity of the diffraction pattern:

$$I(XY) \sim |\Phi(XY)|^2, \quad I_H \sim |\Phi_H|^2. \qquad (38)$$

The second expression is written for a crystal. One can observe this diffraction pattern on the screen of the instrument by putting the projection system of lenses into a regime in which it transfers to the screen not the image plane of the objective lens, as in Fig. 5a, but its back focal plane (Fig. 5b). This mode is called the microdiffraction mode, since one can

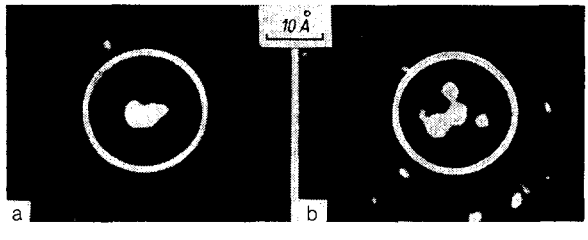

FIG. 13. A df image of clusters of several Au atoms.[48] b—Decomposition of the cluster. The interval between Figs. 13a and 13b is 30 s.

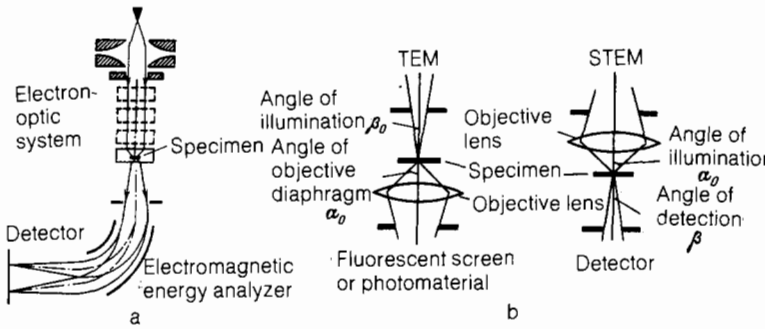

FIG. 14. a—Schematic diagram of a scanning electron microscope. b—Equivalence of the diagrams of the TEM and the STEM.

use a selector diaphragm to select in the intermediate image any microregion of the specimen being studied and obtain diffraction from it, and further, if needed, an image.[23,26]

The em observation of microdiffraction and the measurement of the position of the diffraction maxima make it possible to determine exactly the periodicity and superperiodicity existing in the object (and this implies also the unit-cell parameters of the structure and the superstructures). Measurement of the intensities enables one to evaluate the nature of the diffraction (kinematic or dynamic), the thickness of the specimen, etc. And the use of the set of intensities of the reflections for structure determination is now the object of electron-diffraction structure analysis (EDSA); see below.

3.8. Scanning transmission electron microscopy (STEM)

In addition to the classical scheme of transmission electron microscopy (TEM), there is another scheme—scanning transmission electron microscopy (STEM).[49–51] In SEM a very thin electron beam is formed by a lens system from the electrons emitted by the cathode (one uses field-emission point cathodes). The scanning of the specimen with this beam, which is performed with a step of the order of the cross-section of the beam, and the measurement of the total scattered intensity with subsequent display of each "point" on a television screen yields the image of the object in the form of a raster (Fig. 14a).

In an ordinary reflection SEM one examines massive specimens and studies the spectra of the reflected secondary electrons, Auger electrons, x-rays and photoemission. This enables one not only to characterize the structure of the surface with a resolution of 30–100 Å geometrically, but also to determine the local chemical composition, the character of the chemical bonding, etc. Here one can display on different screens simultaneously both the "ordinary" em pattern and the pattern of distribution of some particular element in the specimen. The chemical composition of the specimen at any selected point is directly displayed.

In the STEM the beam focused on the specimen and transmitted through it has a diameter down to 3–5 Å. Evidently in the STEM the diameter of the beam determines the resolution of the em image.

Since one determines (integrates over all angles) *all* the intensity scattered at a given point, high-resolution STEM is the most sensitive method for detecting individual atoms. But one can measure not only the integral scattering intensity of a point of the specimen, but also the scattering in any angular interval—near the primary beam or only of the deflected electrons. Evidently this is equivalent to the df method in SEM. Moreover, one can analyze the transmitted beam with respect to energy, i.e., measure the elastic and inelastic components. High-resolution measurement of x-ray spectra cannot be performed in practice (capture an x-ray quantum from a single atom!), but this is possible at low resolutions.

At first glance the STEM seems to be a completely different system from the TEM. However, a simple geometric consideration (Fig. 14b) shows that these two schemes are mutually reversed, so that the angle of convergence of the probe α_0 on the specimen is equivalent to the aperture angle of the TEM, while the divergence angle of the probe at the entrance into the detector is equivalent to the angle of "illumination" of the specimen in the TEM. The resolution is determined by the condition (1), $d = 0.61\lambda/\alpha_0$ for $\alpha_0^4 = 4\lambda/C_s$, so that

$$d = 0.43 C_s^{1/4} \lambda^{3/4}. \tag{39}$$

The best resolution attained by Crewe[49] is 2.5 Å. Images of heavy atoms have been obtained by using a STEM with a resolution of 2.5–4 Å, both isolated and contained in an organic molecule (Fig. 15; see also below, Fig. 25). The nano-

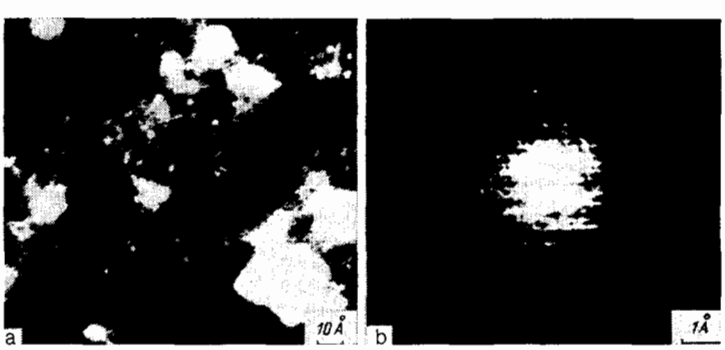

FIG. 15. a—STEM image of Au atoms and clusters on a thin carbon substrate in an $AuCl_3$ preparation. b—Densitogram of the image of a single atom with a peak half-width about 2 Å.[49]

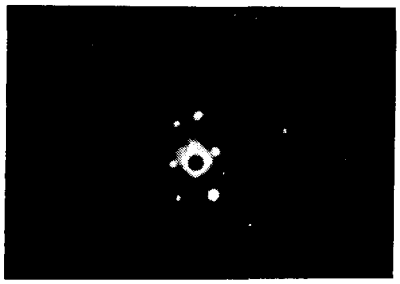

FIG. 16. Nanodiffraction pattern of a particle of bismuth molybdate 8 nm in diameter.[53]

diffraction patterns in such a sharply convergent beam are of great interest.[52] (They are called this because one can observe regions of dimensions 2–20 nm (Fig. 16). These patterns prove sensitive to differences in the structure of a crystal comparable in magnitude with the dimensions of unit cells. The diffraction reflections themselves also have a complex structure.

3.9. EM Images of atoms

We have already seen (see Figs. 12 and 15) that one can observe individual atoms in the electron microscope. But what actually do we see in such an image? The scattering from an individual atom is described by the general formula (7a), (7b). If further we take account of the spherical symmetry of an atom, we obtain an expression for the absolute magnitude of the atomic scattering amplitude in the Born approximation:

$$f_{\text{el}}(s) = \frac{2\pi me}{h^2} \int \varphi(r) \frac{\sin(sr)}{sr} \cdot 4\pi r^2 \, dr \qquad (40)$$

($s = 4\pi \sin\theta/\lambda$). Although electrons are scattered by matter considerably more strongly than, e.g., x-rays are,[17] the absolute magnitude of the scattering of the primary wave by an atom turns out to be relatively small. Thus, for example, the total cross section for scattering by an atom with $Z = 20$–30 amounts to about 10^{-2} Å^2. Hence one can obtain an em image of individual atoms. The image in the electron microscope is determined by the projected potential of the object. Therefore, let us examine first the characteristics of the projected potential of an atom φ_{at}.[17] This projection is determined by the atomic scattering amplitude (40), but also, for real objects one should also take account of the thermal motion of the atoms on the substrate, which is described by the Debye-Waller temperature factor:

$$f_{\text{el}\,T} = f_{\text{el}} \exp\left[-B\left(\frac{\sin\theta}{\lambda}\right)^2\right]; \qquad (41)$$

here $f_{\text{el},T}$ is the atomic temperature amplitude—the scattering from the "vibrating" atom. The quantity B equals $8\pi^2\bar{u}^2$, where $\bar{u}^2$ is the mean-square displacement of the atom from the equilibrium position. The magnitude of the displacement $(\bar{u}^2)^{1/2}$ depends on the strength of the bonding of the atom with the surrounding atoms (in a molecule, on a substrate, in a crystal) and their atomic number. For heavy atoms we can roughly estimate $(\bar{u}^2)^{1/2}$ as ~ 0.1 Å or less, i.e., B is near 0.5–1; for organic materials we have $B \approx 3$–4. Let us examine the projection of the potential of an atom $\varphi_{\text{at}}(u)$. It is determined by the plane Fourier-Bessel transform of (41):

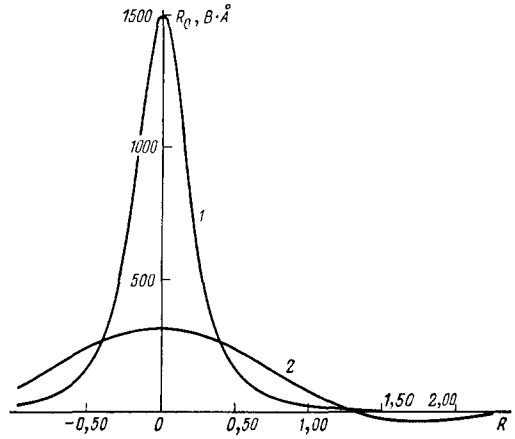

FIG. 17. Ideal and real em images of the projected potential of a gold atom. Curve *1*—distribution of the projected potential of Au for $B = 1$, *2*—convolution of this distribution with the transform of an aperture of radius $U_{\max} = 0.5$ Å^{-1}; one sees that this real image of the spot from the Au atom is determined by the transform of the aperture.

$$\varphi_{\text{at}}(u) = \frac{1}{2\pi} \int_0^\infty f_{\text{el}\,T}(s)\, s J_0(sr) ds. \qquad (42)$$

Here J_0 is the zero-order Bessel function.

Figure 17 (curve *1*) shows the projected potential of a gold atom ($Z = 79$) "blurred" by thermal motion (for $B = 1$). This is a rather sharp function with a half-width about 0.7 Å. In estimating how the atom appears in an electron micrograph, two quantities are of interest: the height of the peak of the potential

$$\varphi_{\text{at}}(0) = \frac{1}{2\pi} \int_0^{s_{\max}} f_{\text{el}}(s)\, s\, ds \approx 57\ Z^{0,75} q(s_{\max})\ (\text{V}\cdot\text{Å}) \qquad (43a,b)$$

and the integral of $\varphi_{\text{at}}(u)$, the "total potential" of the atom[17]:

$$\varphi_{\text{at,tot}} = \int_0^\infty \varphi(u) \cdot 4\pi u\, du \approx f_{\text{el}}(0) \approx 183 Z^{1/3}\ (\text{V}\cdot\text{Å}^3). \qquad (44a,b)$$

The values of $\varphi_{\text{at}}(0)$ are calculated in Ref. 54. The quantity $\varphi_{\text{at}}(0)$ depends on the thermal motion, which blurs the peak and diminishes its height. The values of the coefficients in (43b) for $\varphi_{\text{at}}(0)$ are given for $B = 1$. The quantity $q(s_{\max})$ takes into account the effect of the aperture; it also diminishes the peak height. For $U_0 \approx 0.5$ Å^{-1} we have $q \approx 0.3$. For an Au atom with $B = 1$ we find $\varphi_{\text{at}}(0) = 1500$ V·Å.

The total potential $\varphi_{\text{at,tot}}$ of (44) is nothing other than $f_{\text{el}}(0)$, and this quantity determines the integral "brightness" of the atom in the df image. Naturally, both $\varphi_{\text{at}}(0)$ and $\varphi_{\text{at,tot}}$ increase with Z, the peak height being more sensitive to Z. It is practically almost impossible to detect isolated light atoms with $Z < 20$ in the EM. The medium atoms ($Z \approx 30$–40), and of course, the heavy atoms—Au, Hg, V, Th—are reliably manifested. An atom is a weak phase object, and according to (36), in bright field we have

$$I_{\text{bf}} = 1 + d(u) * 2\sigma\varphi_{\text{at}}(u). \qquad (45)$$

The intensity from an atom is

$$I_{\text{at}} \sim d(u) * \varphi_{\text{at}}(u). \qquad (46)$$

The half-width of the peaks $\varphi_{at}(u)$ is about 0.7–0.8 Å. However, unfortunately the blur function $d(u)$, which has a half-width about 2 Å in the best instruments (1.5 Å for megavolt microscopes), is found to leave little of the intrinsic distribution φ_{at} in the image; the total half-width is about $(2^2+0.7^2)^{1/2}\approx 2.1$ Å—this is mainly $d(u)$ itself (see Fig. 8). In addition to the main peak, the latter has side maxima that are practically lost in the background. Thus the "atom" is visible, but as a spot of form approximating $d(u)$ (see Fig. 17, curve *2*). This function determines the shape of the peak, while, depending on the atomic number, its height is given by Eqs. (43) and (44) with allowance for the effect of the aperture on the height of a peak of magnitude q. The dependence of the image intensity on Z can be modeled on a computer, but in the most exact studies up to now, this dependence has not been measured experimentally.

The actual contrast of the bf image is determined by the relationship of the useful signal to the background from the substrate (carbon film), the "noise" of the photomaterial or detector, etc., and of the "bright" field. For gold atoms in the range of accelerating potentials 100 kV–1 MV, the contrast is estimated to be 20–30%.[22] The image of an atom appears here as a scattering deficit on the bright field from the primary beam. Figure 18 gives an example of this type of image.

The dark-field method is more favorable for detecting individual atoms. As we have already said, owing to the absence of the bright field, in it the atoms themselves seem to "glow" by the radiation that they have diffracted—these are bright spots on a dark background (see Figs. 12, 13). Here there is no interference with the primary wave, the intensity is proportional to the square of the amplitude, and according to (37), we have

$$I_{df,at} = d^2(u) * (\sigma\varphi_{at})^2. \tag{47}$$

The term $\bar{\varphi}$ in (37) here has practically no meaning. The height of the peak[17] according to (43) is

$$\varphi_{at}^2 \sim Z^{3/2}. \tag{48}$$

As regards the integral brightness of the image of an atom in the df method, according to the Parseval equation[54] it equals the total cross section of the scattering by the atom:

$$2\pi\int_0^\infty \varphi_{at}^2(u)u\,du = \frac{1}{2\pi}\int_0^{s_{max}} f_{el}^2(s)\,ds \sim 0.9Z^{1,27}q. \tag{49}$$

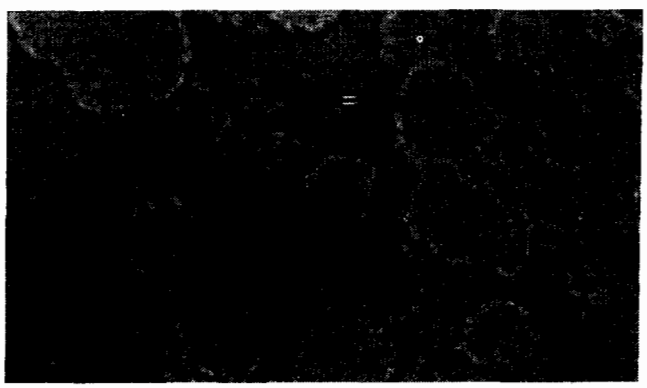

FIG. 18. Bf image of individual atoms and clusters of W on a thin carbon substrate.[22]

Here the coefficient q is close to unity (about 0.9) owing to the rapid decline of the f^2 curve with increasing s.

In the df method the atom appears as a spot of form $d^2(u)$, but with a different dependence of the intensity on the atomic number than in the bf method. The df method is more convenient for revealing isolated atoms than the bf method, and specifically it (and especially the SPEM method equivalent to it) [Translator's note: SPEM is an unfamiliar abbreviation not defined in this article, but the context suggests: dark-field STEM.] is most often used to obtain images of isolated atoms (see Figs. 12, 13, 15).

Let us study the problem of the images of ionized atoms. As is known, the atomic scattering amplitude f_{el} for electrons (42) is related to the atomic scattering amplitude f_{xr} for x rays by the electron density of the atom by the relationship

$$f_{el}(s) = (8\pi^2 me^2/2h^2)(Z - f_{xr}(s))/s^2. \tag{50}$$

Here Z is the charge of the nucleus creating the Coulomb potential, and f_{xr} describes the screening effect of the electron shells; $f_{xr}(0) = Z'$ is the negative charge of the electron shell. For neutral atoms we have $Z = Z'$, and f_{el} has no singularities at low angles. Yet for ions, for which $Z - Z' = n \neq 0$ (the charge of the ion is positive or negative), (50) is inapplicable—it goes to infinity, while actually f_{el} near small angles becomes very large. Estimates show that the scattering power of ions exceeds by a factor of ten or so the scattering power of neutral atoms.[17,55] We note that a certain deviation from Eq. (40)—the first Born approximation—occurs for the heaviest atoms.[56]

This is described by adding an imaginary component to f in (40):

$$f = f' + if''. \tag{51}$$

Actually this small increment is of no significance in the formation of the em image of atoms: roughly speaking, what is lost in phase contrast goes into amplitude contrast. However, by using (33) one can take account of such an "absorption" arising from μ_{at}.

3.10. EM images of crystal structures. Thin crystal

Already geometric considerations show that the thinner a crystal is, the easier is it to obtain an em image from it.[57] This involves the realization of the possibility of appearance of high-order diffracted beams. The wavelength λ is finite, and the approximation of a "plane" Ewald sphere (see Fig. 6) for large H is not valid. The sphere deviates from a plane with increasing H, and to obtain an image of a lattice, it is necessary that it be formed from, at least, several beams. That is, the sphere must intersect several nodes H_{hk0}. The form of a node in the z direction is given by the Laue function $\delta(A,z) = \sin(\pi Az)/\pi z$, and its half-width is A^{-1}. The Ewald sphere at the distance H from the origin deviates by $s_H = H^2\lambda/2 = \lambda/2d^2$ from the plane, and for it to "catch" the node H, we must have $s_H < 1/2A$. That is, the thickness of the crystal must be

$$A < \frac{d^2}{\lambda}. \tag{52}$$

Here d is the "interplanar spacing" of the limiting reflection. Thus, to obtain a resolution of 2 Å, we must have $A < 100$ Å.

On the other hand, the condition that the object be a

weak phase object is *per se* a condition of small thickness of the crystal. The kinematical structure amplitude is determined by the scattering from an atom of the crystal with account taken of its coordinates $\mathbf{r}_i$ in the unit cell:

$$\Phi_{\mathbf{H}} = \sum_i f_i \exp(2\pi i \mathbf{r}_i \mathbf{H}). \tag{53}$$

In kinematic scattering these amplitudes must be weak in comparison with the amplitude of the primary wave. The intensities I_H of the scattered beams in the kinematic theory are determined by the formula[17]:

$$\frac{I_H}{J_0 S} = \lambda^2 \left| \frac{\Phi_{\mathbf{H}}^{\text{abs}}}{\Omega} \right| A^2. \tag{54}$$

Here $J_0 S$ is the primary intensity incident on the crystal of area S, and A is the thickness of the crystal. The condition of kinematicity of scattering is the condition of smallness of (54), whence we have

$$A < \lambda \overline{|\Phi^{\text{abs}}|}\, \Omega^{-1} = A_{\text{cr}}. \tag{55}$$

Here $|\Phi^{\text{abs}}|$ is the mean absolute value of the strongest amplitudes $|\Phi_{hk0}^{\text{abs}}|$, and Ω is the volume of the cell. For structures made of light atoms the critical thickness (extinction length) A_{cr} amounts to ≈ 200 Å; for atoms of medium atomic numbers $A_{\text{cr}} = 50$–100 Å; and for crystals made of heavy atoms $A_{\text{cr}} < 50$ Å. In these cases the condition of a weak phase object (14) is fulfilled and the formation of the image of crystals is described by Eqs. (14) and (15).

Upon increasing the thickness of specimens, especially those consisting of heavy atoms, the effective absorption—the second terms of Eqs. (18) and (19) yielding the amplitude contrast—play an ever greater role. We must also note that, owing to the angular dependence of the atomic scattering factors and the influence of the aperture that cuts off part of the scattered radiation, the observed contrast can be partly interpreted as amplitude contrast.[11,26] When one uses the bf method, according to (36), for thin crystals having columns of atoms projecting on one another in the direction of the primary beam and having the two-dimensional coordinates $\mathbf{r}_i$ in projection, we have

$$I_{\text{bf}} = 1 + d(u) * 2\sigma \sum_i n_i \varphi_{\text{at},i}(\mathbf{r} - \mathbf{r}_i)\, D(xy). \tag{56}$$

For crystals the function $\varphi(xy) = \Sigma \varphi_{\text{at},i}$ is periodic, and this is a Fourier series in the amplitudes Φ_{hk} of the beams passing through the aperture:

$$\varphi(xy) = \frac{1}{S} \sum_{h,k} \Phi_{hk} \exp\left[2\pi i \left(\frac{hx}{a} + \frac{ky}{b}\right)\right] \tag{57}$$

Φ_{00} enters into the first term, which is unity in (56). The function φ in (56) is bounded by the form $D(xy)$ of the projection of the crystal, while the possible differences in thickness are taken into account by the number n_i of atoms in the projection. As we know, the form of the spots from the atoms is determined by the blur function $d(u)$. It is possible to resolve atoms in the crystal if the half-width of $d(u)$ is smaller than the interatomic spacing (see Fig. 8). If the individual heavy atoms in the crystal lie far from one another or are surrounded by light atoms and are thus "moved apart," the requirements on the resolution are lowered (see Figs. 4 and 12). Pairs of close-lying atoms at insufficient resolution appear as a single spot (see below, Figs. 32 and 37).

At even lower resolution all the φ_{at} of (56) merge, and now the mean internal potential φ is significant. On its background structures coarser than atomic, but still microfeatures, can be manifested by phase or amplitude contrast, e.g., inclusions of foreign phases, crystal-structure defects such as dislocations, etc.[27]

We note that Eq. (56) is also suitable for describing images of molecules, but without n_i and D. When needed, we can also take absorption into account in (56), assuming that φ_{at} contains also an imaginary component μ_{at}, as in (18): actually the absorption mainly involves the interaction of the incident electrons with the electrons of the object concentrated in the atoms. In the dark-field method for a thin crystal, according to (37) and analogously to (56) and (57), we have

$$I_{\text{df}} = \sigma^2 d^2(u) * \left[\sum_i n_i \varphi_{\text{at},i}(\mathbf{r} - \mathbf{r}_i)\right]^2 D(xy), \tag{58}$$

or, upon expanding φ in a Fourier series,

$$I_{\text{df}} = \sigma^2 d^2(u) * \left\{ n \sum_{h,k}{}' \Phi_{hk} \exp\left[2\pi i \left(\frac{hx}{a} + \frac{ky}{b}\right)\right]^2 \right\} D(xy); \tag{59}$$

the term Φ_{00} is absent in (59). Obtaining images of thin crystals by the df method as compared with the bf method does not possess such evident advantages as for individual atoms, since the contribution of the terms yielding the image of the structure in (56) is comparable with unity, or with the bright field.

Let us examine the case of formation of a bf image of a crystal from only two beams—the primary beam (which contains also Φ_{000}) and one scattered beam (e.g., Φ_{220}) having the interplanar spacing d_{220}. This will seemingly yield the Fourier synthesis from only the zero and one other harmonic, and the distance between the bands will be d_{220} (Fig. 19). This is just what was observed in the first em images of "crystal planes" (see Fig. 2). Even in the case of thick crystals, for which the correct phase relationships and intensities of the zero-order and one scattered beam do not correspond to the same for the kinematic amplitudes, the existence of any phase shift will lead to the imaging of lattice bands, or "planes," but the intensity distribution does not correspond to the actual scattering power. To observe the projection of the atomic structure of crystals in the HREM, both in the bf

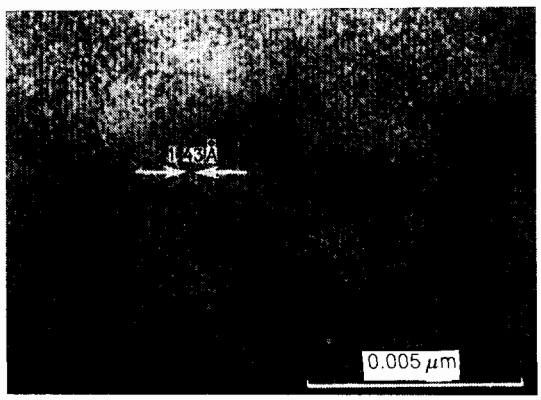

FIG. 19. Image of the (220) "crystal planes" of the structure of gold.[40]

and the df methods, one must include in the formation of the image the entire two-dimensional system of diffracted beams Φ_{hk0} transmitted by the optimal aperture (see Fig. 7). For this reason obtaining the images of crystal structures with high resolution is sometimes called "many-beam" EM, although this is not fully exact, since not only the diffracted beams ("rays") participate in image formation, but the entire diffraction field between them. In principle one can eliminate the difficulties occasioned by allowing for Φ_{00} by using a *partial* screening of the primary beam—this would seem to be a combination of the bf and df methods.

3.11. EM images of thick crystals

The kinematic approximation, and correspondingly, the weak-phase-object approximation, is inapplicable for crystals whose thickness $A > A_{cr}$ (55). Each scattered beam that has arisen in the crystal can itself be treated as a primary beam, undergo diffraction, and interfere with the primary and other beams that have arisen (and they with it and among themselves). At the exit from the crystal it has an amplitude and phase differing from those given by (53). This treatment serves as an example of the dynamic theory of electron scattering, the basis of which was founded by Bethe[30] and which has been developed further in a multitude of studies (see Refs. 11, 31, 32, 59–62). This theory has much in common with the dynamic theory of x-ray scattering.[58]

Let us denote by ϕ_H the dynamic scattering amplitudes of the beams $H = h, k, l$ (they do not coincide with the kinematic Φ_H (9a, 53), but depend on them). Depending on the mutual orientation of the crystal and the primary beam, i.e., the position of the ideal point nodes H of the reciprocal lattice with respect to the Ewald sphere, scattered beams ϕ_H are excited whose nodes exactly coincide or are close to the sphere. The parameter of closeness is the distance s_H of the node from the sphere ("excitation error"; see Fig. 6). If a primary beam having the unit amplitude $\Phi_0(0)$ is incident on a plane-parallel plate of thickness A, then we have all the $\phi_H = \phi_H(A)$. The set of n beams that arise obeys the condition of conservation of intensity—it can only be "pumped" from beam to beam:

$$\Phi_0(0)\,\Phi_0^*(0) = 1 = \sum_{i=0}^{n} \Phi_{H_i}(A)\,\Phi_{H_i}^*(A). \qquad (60)$$

If we construct the scattering matrix[63,64] from the absolutized kinematic amplitudes $v \to v_H = 4\pi K \Phi_H$,

$$\exp\left(i\frac{MA}{2x}\right), \quad M = \begin{pmatrix} P_0 & \dots & v_{0H} & \dots & v_{0G} \\ v_{HA} & \dots & P_H & \dots & v_{HG} \\ \cdot & \cdot & \cdot & \cdot & \cdot \\ v_{G0} & \dots & v_{GH} & \dots & P_G \end{pmatrix}, \qquad (61)$$

then the solution is given by the relationship

$$\begin{bmatrix} \Phi_0 \\ \cdot \\ \cdot \\ \cdot \\ \Phi_G \\ \cdot \\ \cdot \\ \cdot \\ \Phi_H \end{bmatrix} = \exp\left(i\frac{MA}{2x}\right) \cdot \begin{bmatrix} \Phi_0(0) \\ \cdot \\ \cdot \\ \cdot \\ 0 \\ \cdot \\ \cdot \\ \cdot \\ 0 \end{bmatrix}. \qquad (62)$$

The diagonal terms are $P_H = 2KS_H$, $K = (v\varkappa_0^2 + v_0)^{1/2}$, where K and $\varkappa_0$ are the magnitudes of the wave vectors of the incident wave in the crystal and *in vacuo*, and v_0 in the mean internal potential.

A very simple case is the two-wave case, in which one strong scattered beam is excited in addition to the primary beam. Here, as the wave passes through the crystal, alternate pumping of intensity occurs from Φ_0 to Φ_H and back (pendulum solution). In this case the em image (as in the kinematic treatment) is the image of the lattice planes perpendicular to H with varying contrast. In the case in which many beams arise, depending on the thickness of the crystal and the parameters of the transfer function, the em image corresponds only in individual cases to the "image of the atomic structure," but most often a pattern arises that is determined, of course, by the structure, but does not directly match it. In these cases one must calculate and model the image.

The calculation of images of thick crystals is performed

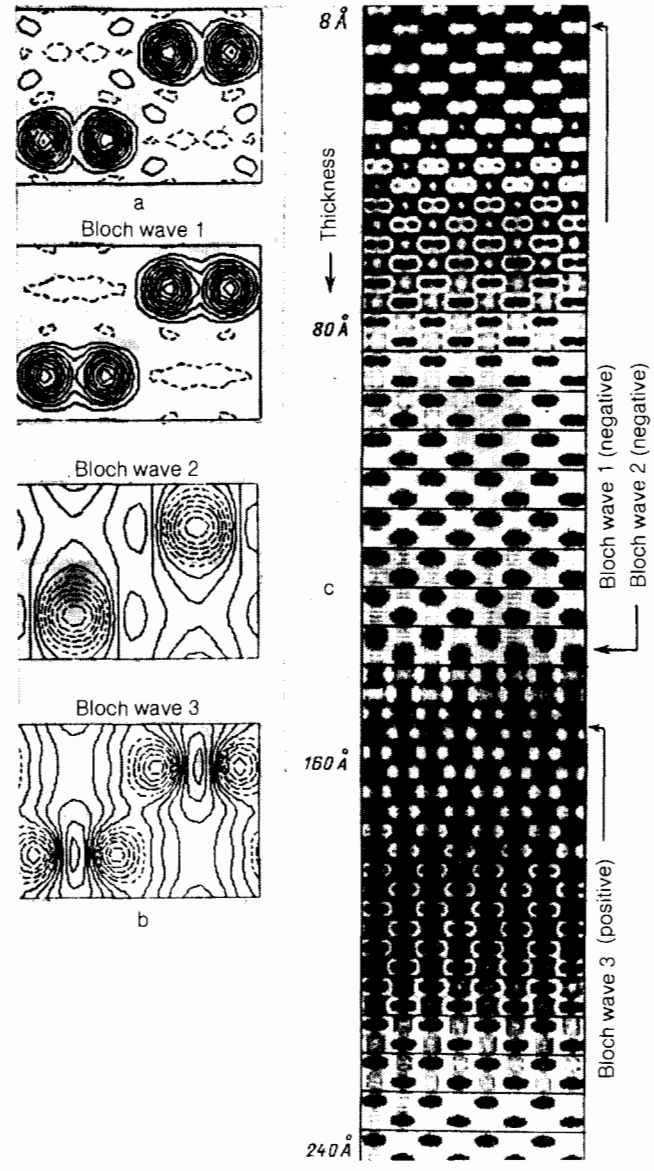

FIG. 20. Image of Ge atoms in the crystal as a function of thickness (calculated).[68] a—Projected potential. b—Three fundamental Bloch waves, the first of which is excited at the smallest thicknesses of the crystal and practically coincides with the projected potential. c—Calculation of the observed pattern as a function of thickness. The Bloch waves evolve; *1* evolves into *2*, and *2* into *3*; contrast reversal occurs.

either directly with the formulas of the dynamic theory, or with an interpretation of it using Bloch waves, or by the phase-lattice method. Concepts are also used that are based on the channelization approach.[65]

The system of waves established in the crystal in dynamic scattering is a certain wave field that (especially for simple structures) is conveniently interpreted by using Bloch waves, which automatically take account of the periodicity of the lattice.[66,67] The set of amplitudes ϕ_H corresponding to a certain dynamic solution yields the Bloch wave

$$\Psi^i(\mathbf{r}) = \sum_j \Phi^i_{H_j} \exp(iK^i_{H_j}\mathbf{r}). \quad (63)$$

It turns out, for example, that three fundamental Bloch waves are established in a germanium crystal upon passage of a primary wave along [110] (in taking account of the beams). One can describe the em image, depending on the thickness, as the image of one of these three waves. As the thickness is increased, identical images periodically repeat, while contrast reversal occurs at certain thicknesses (Fig. 20).[68,69]

Taking account of dynamic effects is absolutely necessary in analyzing em images of crystal defects, in treating extinction phenomena in diffraction from bent crystals, wedge-shaped edges of crystals, etc. In these cases, as a rule, atomic resolution is not used, yet the observed patterns yield valuable information on the violations of the ideal structure.

3.12. The phase-grating method (layer method)

This method recalls the method of Darwin in the dynamic theory of x rays,[70] in which the crystal is subdivided into "thin" layers, for each of which the kinematic approach holds.

The layer method[11,71] is applied for "strong" phase objects, e.g., those whose thicknesses exceed A_{cr} of (55), but of course, it can be also employed for small thicknesses.

The object is subdivided into layers of thickness Δz having the following projected potential distribution:

$$\varphi_n(xy) = \int_{z_n}^{z_n+\Delta z} \varphi(xyz)\,dz\,. \quad (64)$$

Then one examines the set of N two-dimensional layers spaced apart by Δz. The transmission functions q of (12) and (14) and correspondingly, the phase functions Q of (15) acquire the form

$$q_n(xy) = \exp(-i\sigma\varphi_n\Delta z) \approx 1 - i\sigma\varphi_n\Delta z, \quad (65a)$$

$$Q_n(XY) = \mathfrak{F}q_n = \delta(XY) - i\sigma\Phi_n(XY)\,\Delta z. \quad (65b)$$

In diffraction by a crystal, periodicity exists both in real and in reciprocal space, $Q_n = Q_n(hk)$. On passing the distance Δz from layer to layer, the wave is diffracted, as is described by the convolution of q_n with the propagation function $p_n = ik(x^2+y^2)/2\Delta z$. For N layers we have

$$\psi(xy) = q_N[\ldots[q_1 * [q_0 * p_0] * p_1] * \ldots] * p_n. \quad (66a)$$

In reciprocal space, if $P_n = p_n$, the action of each layer on the wave that has arrived at it from the previous layer is described by the recurrence relationships

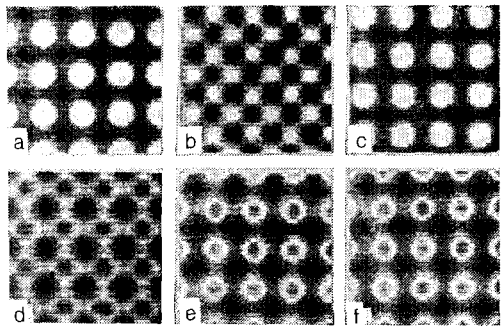

FIG. 21. Calculated images of the [001] projection of the gold crystal.[43] Ten unit cells, thickness 40 Å, $C_s = 1.8$ mm. Defocus Δf(Å)—a: +125; b: +75; c: +25; d: −25; e: −75; f: −125. The contrast is direct at $\Delta f = -25$ Å, reverse at $\Delta f = -125$ Å. At certain values of Δf the images of the projections of atoms are surrounded by halos.

$$\Psi_n(XY) = [\Psi_{n-1}\ P_{n-1}] * Q_n. \quad (66b)$$

To obtain the final pattern of the image, one introduces into the calculation the transfer function T of (20) and (24) for some given defocus. When desired, one can further take account of the amplitude contrast in (65a) and (65b), just as in (18) and (19). As a rule, the calculated images are good models for the observed patterns. In a number of cases they enable one to interpret these patterns correctly, but to do this one must already know the atomic structure. We must note that the phase distortions in dynamic scattering in a crystal, together with their possible distortions in the lens, can sometimes cause the atom spots resolved in micrographs to be shifted from their real positions (see below, Fig. 29b). The calculations confirm the experimentally observed contrast reversal of the images of atoms or atomic groups upon changing the defocus (Fig. 21).

In very "thick" (in the em sense) crystals, interference of inelastically scattered waves plays an ever greater role, which is manifested in diffraction (in electron-diffraction patterns) in the form of the so-called Kikuchi lines and bands. It is practically impossible to observe the atomic structure in these cases.

3.13. The method of staining bioobjects

In analyzing the structure of biological macromolecules and associations of them, e.g., thin crystal layers, tubular crystals, virus particles, etc., one often employs the method of negative staining—immersing the object in a layer of material, e.g., phosphotungstic acid, that strongly scatters electrons. In this case one can interpret the image by using the weak-phase-object approximation,[72] but the amplitude component of the functions (18) and (19) also plays an appreciable role. In this case the electron micrographs depict essentially not the object itself, but the distribution of the stain around or in it (Fig. 22). The attainable resolution of the object here is low (15–30 Å), but by using the method of three-dimensional reconstruction one can obtain valuable information on the spatial structure of protein molecules and other biological objects.[74,75] For unstained biocrystals one obtains diffraction down to 2–3 Å, but an em image at such a resolution has not yet been obtained.[76]

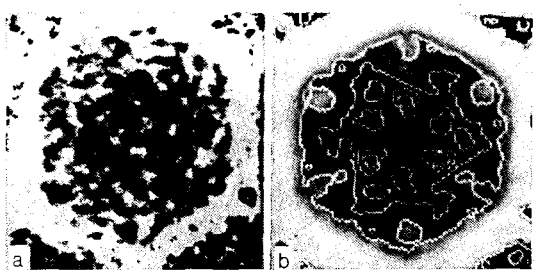

FIG. 22. a—Electron micrograph of carnation ring spot virus—negative stain. b—Image averaged from 64 micrographs in equidensity lines shown on a halftone display.[73]

3.14. Processing, interpretation, and calculations of images

The visible image of an object yielded by an electron micrograph almost always conveys the structure of the object with certain distortions, owing to a number of limitations in the experimental technique and difficulties in obtaining the needed specimens (we recall that we are discussing the atomic and molecular scales). Artifacts can occur. Therefore electron microscopists always remember: "Don't believe your eyes"—think about what you are seeing.

The instrumental imperfections of the image have as their source the electrical, mechanical, and other instabilities of the electron microscope, and imperfections of the optical system. In recording the image the photofilm or other defects introduce their intrinsic noise into it.

One mounts the object in the electron microscope on an amorphous substrate (carbon, organic), which introduces its background into the image. The various methods of specimen preparation can sometimes damage their intrinsic structures (this holds especially for the methods of staining biomolecules). Much unpleasantness is introduced by the contamination of the object and the space around it inside the pole pieces of the objective lens by the residual organic material in the "vacuum" of the instrument. Radiation damage by the incident beam is often substantial.

Various methods of processing and interpreting the images are applied for obtaining qualitative data adequate to the object, and of course, quantitative results.[74,77-80]

The simplest of these, which is applicable to images of objects having some particular symmetry, is optical averaging. For images of crystal structures, this averaging can consist in obtaining a print from a negative that is successively shifted several times by the amount of the lattice period (Fig. 23b–e). If the object has rotational symmetry like certain biostructures (or the same lattice), the averaging can be performed by rotating the negative.

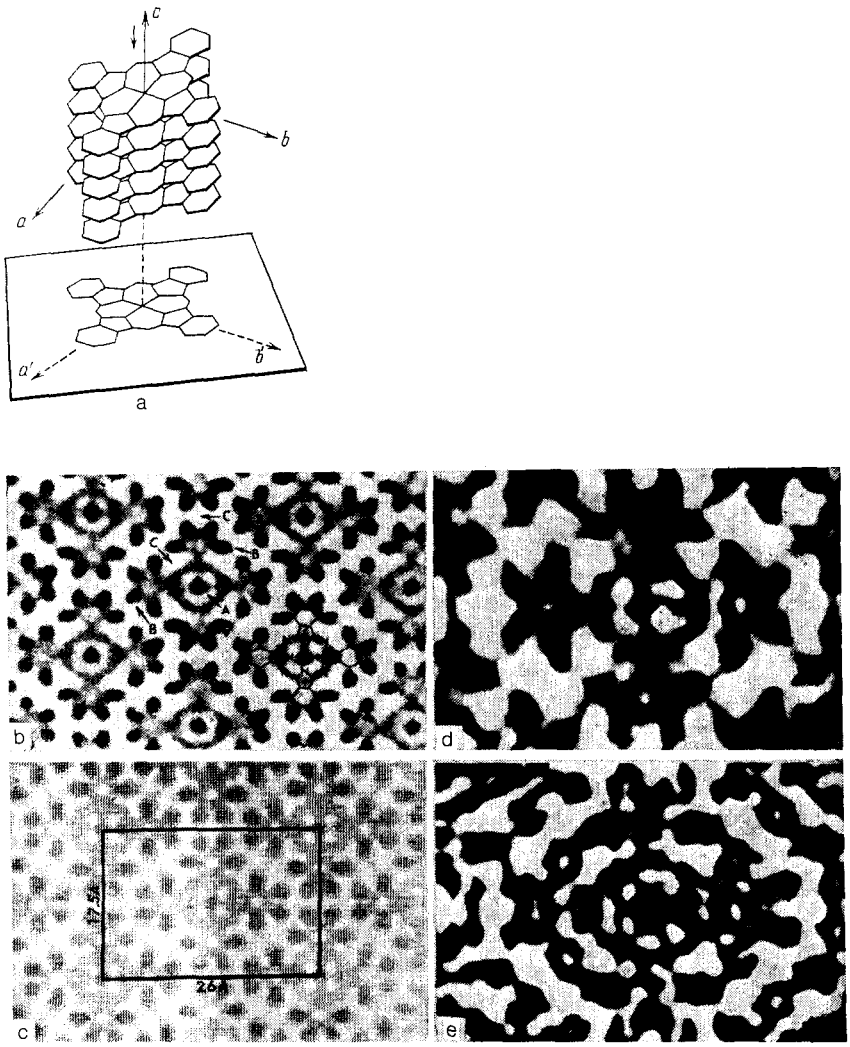

FIG. 23. One of the most interesting em studies of molecular crystals–copper chlorophthalocyanine, performed on the 500-kV electron microscope of Kyoto University. a—Diagram of the packing of molecules in the crystal in stacks that yield a single projection. b—Image of the projection of the crystal showing the "skeleton" of the molecule; the image has been averaged photographically by shifting over the unit cells; *A*—Cu atom, *B*—Cl atoms, *C*—regions of negative contrast around the Cl atoms. c—Computer simulation of the image at the Scherzer defocus $\Delta f = 960$ Å.[81] d, e—The phase component (projection of the potential φ) and the amplitude component (projection of the absorption function μ) separated by computation from the experimental pattern (one unit cell; cf. Fig. 23c). In the projection of the potential the atoms (in particular the C atoms of the benzene rings) are seen most distinctly.[15]

The cited mechanical photomethods are currently often realized by using a computer. First the image is densitometered with special scanning microphotometers with a step of the order of tens of micrometers, and is digitized. The mass of obtained data amounts to from several thousand to several million image pixels. The computer can allow for the sensitometric curve of the photomaterial, remove the background, measure the contrast, etc., and further, if needed, perform averaging and other processing according to a given program and display the result in an exact form (see Figs.22, 23, and below, Fig. 30).

The methods of optical filtration of images of periodic objects are of interest.[82] In the optical diffractometer one obtains a diffraction pattern from the electron micrograph. One can process this image by using the direct ($\mathfrak{F}$) and inverse ($\mathfrak{F}^{-1}$) Fourier transforms of (9a), (10a,b), but on the optical level. This will be $\mathfrak{F}(D)$, where D is the optical density of the negative. If one uses filters to allow only the periodic components of $\mathfrak{F}^{-1}(D) = \Phi_{hk}^{\text{opt}}$ to form the optical image, then all the aperiodic noise will be eliminated. One can transmit only part of the components of Φ_{hk}^{opt} (e.g., if the images of two lattices are mixed), and obtain the image of one of them. This method yields good results in processing images of bioobjects having cylindrical (helical) symmetry. Then $\mathfrak{F}$ and $\mathfrak{F}^{-1}$ are Fourier-Bessel transforms. As was pointed out above, all this can be done more exactly also on a computer after digitization.

The methods of image reconstruction have found further development—mainly for biomolecules—in the method of three-dimensional reconstruction. Here one can obtain a *spatial*, volume picture of the structure of an object from a series of electron micrographs or from a single micrograph, but of a symmetric object.[3)]

In the interpretation of images at the atomic level of resolution, computational model-building plays a great role. The investigator always tries to select the best conditions of photography, defocus, and specimen preparation with a suitable thickness, but one does not know them exactly. One can calculate the image by various methods—construction of the projected potential of (57), the phase-lattice method of (64)–(66), the dynamic theory in the many-beam variant of (62), or a method based on the Bloch approach of (63).

The choice of the parameters of the machine experiment that yields the best approximation to the actually observed pattern thus determines the structure of the actually observed object. Of course, a flaw of this method is the need to have a starting model, i.e., to know the structure to some degree—yet that is what we wish to investigate. However, here one can proceed by the method of successive approximations, analogous to the earlier use of the method of trial and error in diffraction methods of studying atomic structure. The calculations become complicated if one must model a structure having defects or an aperiodic structure.

If the image is obtained under conditions in which several maxima and minima of the transfer function W of (24) fit into the aperture, then, if we know this function, we can eliminate its effect. In the most frequent case in which the fundamental contribution to the image comes from the potential φ, only the sine component $\sin\chi$ of (24) and (38) influences it. In this case one performs the inverse Fourier transformation of (35) and obtains Q' of (33). Then one divides it by $\sin\chi$ and finds Q of (15), while the Fourier transform of Q yields I_{bf} of (35), from which the effect of $\sin\chi$ has been eliminated.

One can find the parameters of the CTF and simultaneously separate the image into its phase (φ) and amplitude (μ) components by the method of through-focus series.[83,84] According to (35), $I(xy)$ depends on both these components and on the defocus (via χ_1) of (25). The contribution of φ and μ is constant, but the defocus can be varied. In principle two different values of it suffice to separate the φ- and μ-components (see Fig. 23). Yet in practice, since the parameters of T are not known exactly, and also owing to the existence of a background, the calculations are performed by the least-squares method.[86] We must note that the contrast transfer function $\sin\chi_1$ can be found from the electron micrograph itself by observing the optical diffraction pattern—it is revealed in the annular modulation of the image from the amorphous substrate or, if the object is crystalline, from the noise component of the image.

The methods of densitometry of electron micrographs and subsequent processing and modeling can be replaced by recording systems directly built into the electron microscope (on-line) that are linked to a computer. Such systems already exist in a number of laboratories. They include a receiver of the image of the object or its diffraction pattern of the vidicon type, with output on a display, digitization of the image and measurement of diffraction intensities, computer algorithms for direct and inverse Fourier transformation, for methods of averaging and filtration, calculation of the image for different defocuses, methods of correlation of observed and calculated patterns, etc. All this makes it possible to obtain the most complete and accurate information on the object of study directly in the course of an experiment.

Electron microscopy proper is supplemented by the analytical em methods. For example, STEM enables one to determine the local chemical composition from the characteristic x-ray radiation, while a number of potentialities are opened up by energy analysis of scattered electrons.

3.15. Comparison of the potentialities of electron microscopy and diffraction structural analysis of crystals

In electron microscopy the image is formed from the diffracted beams, which physically undergo the double Fourier transform of (4) with allowance for the phases of the scattered waves, but they are distorted by the transfer function. In electron-diffraction structural analysis (EDSA)[17] and the more widely applied x-ray structural analysis,[87] as well as neutron diffraction,[88] one measures the intensities of the scattered beams $I_H \sim |\Phi_{\mathbf{H}}|^2$ of (38), finds from them the moduli of the scattering amplitudes $|\Phi|$, determines their phases (which are not determined experimentally) by calculation, and constructs a Fourier synthesis by inverting (7a):

$$\frac{1}{\Omega}\sum_{\mathbf{H}} \Phi_{\mathbf{H}} \exp(-2\pi i \mathbf{H}\mathbf{r}) = \varphi(\mathbf{r}). \qquad (67)$$

This expression is written for EDSA, in which we obtain the potential distribution (Fig. 24a) on the basis of the electron reflections (Fig. 24b). In EDSA one employs special apparatus—electronographs, in which there are no lenses afer the specimen, and one can directly, without distortions, record the diffraction pattern and measure the intensities I_{hkl} exactly. One can do this also by using an electron microscope in

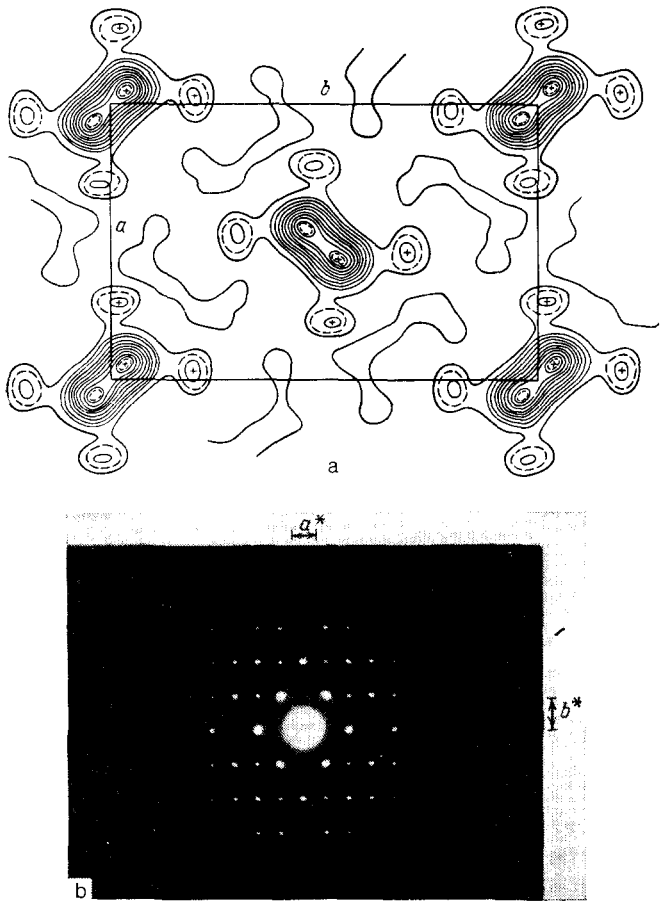

FIG. 24. Fourier synthesis of the projected potential of the structure of paraffin (a) constructed from the amplitudes of the $hk0$ reflections present on the electron-diffraction pattern (b).

the diffraction mode. Analogously to (67), x-ray diffraction enables one to obtain the distribution of electron density $\rho(\mathbf{r})$, while neutron diffraction determines the nuclear scattering density or the density of magnetic moments. The optical system of the microscope is replaced in structural analysis by mathematical summation of Fourier series. This is now not a "physical microscope," but a "mathematical" one. The potentialities of this microscope are very great—resolution down to 0.5 Å with complete absence of apparatus distortions apart from truncation of the series. By using it one can determine the coordinates of atoms to an accuracy as great as 0.0001 Å, the parameters of anisotropic thermal motion, and the distribution of electrons or potential in atoms and between atoms. This enables one to obtain the characteristics of chemical bonds. The fact is also very important that the function thus obtained is three-dimensional. That is, it gives the actual volume distribution of the scattering power of the atoms, rather than a two-dimensional projection, as in the TEM. Thus, diffractional structural analysis has undoubted advantages over HREM, which yields the images of atoms as "spots." In measuring the latter, one can say almost nothing about the intrinsic structure of the atoms (besides their relative scattering power). The main information that one obtains in HREM is the information on the mutual arrangement of the atoms or groups of them with an accuracy of determining distances in projection of 0.1–0.2 Å.

However, apart from the incomparably greater laboriousness of experimentation, diffraction structure analysis has its fundamental limitations. First, there is the need for determining the phases of the structure amplitudes by calculation. The current state of the theory enables one to do this in most cases of practical importance, but yet the phase determination for complicated structures remains a difficult problem.[89] The second—and more important—limitation is that the structure analysis of crystals enables one to obtain a pattern of the arrangement of atoms and of their scattering density only in the unit cell *averaged* over the entire structure. Diffraction structural analysis of imperfections of structure at the microlevel (but not at the level of atomic resolution) also functions, but it is no longer a direct method of imaging these imperfections.

At the same time, electron microscopy, in addition to the advantages of perspicuity and speed, enables one to obtain an image of the arrangement of the atoms of a structure, and not only a crystalline one, with all its defects and imperfections, with fixation of implanted atoms, vacancies, and superstructures, and it also allows one to observe atoms in an amorphous structure, etc. In fact, as we have already said, in structural analysis one uses for constructing a Fourier synthesis only the purely periodic component of the scattering pattern—the discrete "point" values of Φ_H of (9b), whereas in electron microscopy the entire scattering amplitude (included in the aperture angle) $\Phi(XY0)$ of (15) is formed and transformed by the optical system, including both the periodic component of (9b), if it exists, and the form of the reciprocal-lattice nodes D (and in consequence they yield the external form of the object in the image formation), and the aperiodic component between the nodes. Though small in intensity, the latter contains precisely the information about the aperiodic perturbations of $\varphi(xy)$. In a number of cases the speed of image recording enables one to observe the structure in dynamic processes, e.g., crystal growth and attachment of new atoms to their surfaces (see below, Fig. 47—video recording), processes of atom migration, rearrangement of a structure in phase transitions and upon irradiation and other actions.

It seems highly promising to combine HREM and EDSA. Then one can determine from the image of the structure (however crude) the phases by calculation, and then assign them to the experimentally measured moduli $|\Phi_{hk0}|$. A beautiful example of this approach is the study of biomembranes.[90]

4. EXPERIMENTAL STUDIES OF ATOMIC STRUCTURE USING HREM

Numerous experiments and calculations confirm the possibility of direct em observation of the structure of matter on the level of atomic resolution and yield a body of new information on the ideal and real structures of crystals and molecules. The content of these studies is best of all embodied in the obtained electron micrographs. Therefore this part of the review will be a narrative to a lesser degree, but to a greater degree a demonstration of images of matter at the atomic-molecular level.

4.1. Images of atoms and molecules

Electron micrographs of isolated atoms and atoms in molecules (see Figs. 12, 13, and 15) yield information on their arrangements. Pictures of this type taken at intervals of

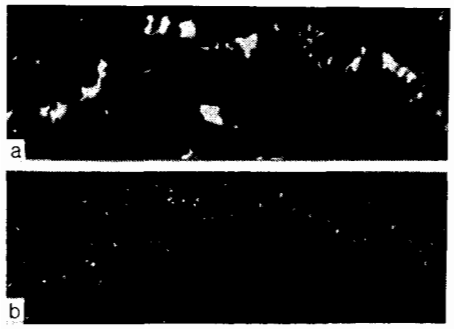

FIG. 25. a—Direct STEM image of Os atoms in a polyuridylic acid chain. b—Filtered image with removal of the low spatial frequencies.[85]

fractions of seconds or seconds (see Fig. 13) show migrations of atoms on the substrate under the action of the electron beam.

One can use heavy atoms for marking molecules of synthetic or natural molecules. This makes it possible, e.g., to study the distribution of certain nucleotides along polynucleotide chains or DNA, or amino acids along the polypeptide chains of proteins. Figure 25 is an image of polyuridylic acid [Translator's note: the original has "polyuranyl," an apparent misreading of the abbreviation "poly U".] labeled with OsO_4-bipyridine. The distance between closest osmium atoms is about 4Å. Figure 26 shows the df TEM image of another molecule containing heavy atoms. In obtaining this type of images, one uses microphotometric and computer processing of the micrographs; as a rule, the light atoms are not resolved. Figure 27 shows an electron micrograph of a large organic molecule consisting of light atoms as well as its iodinated analog.[91]

An excellent example of an image of molecules in a crystal is the already described micrographs of chlorinated copper phthalocyanine (see Fig. 23). In studying larger

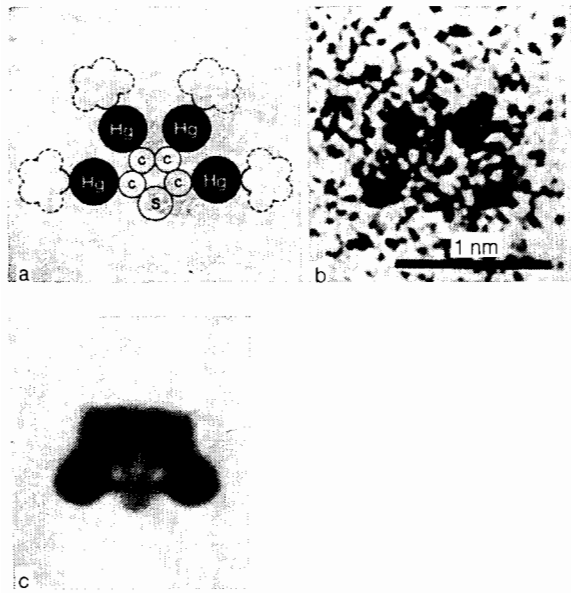

FIG. 26. a—Diagram of the molecule 2,3,4,5-tetraacetoxymercurithiophene. b—Direct df STEM image. c—Computer filtration of the image. The dotted line indicates the acetate groups.

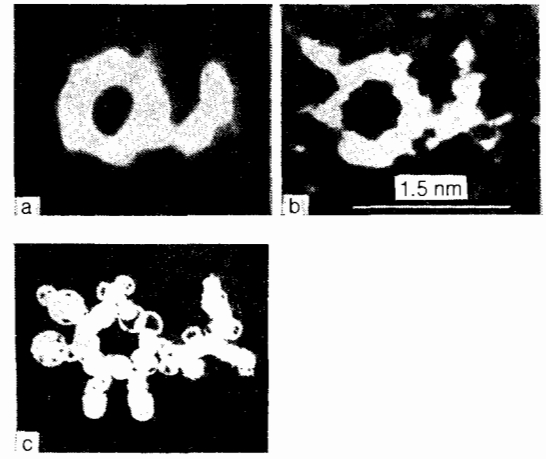

FIG. 27. a—Averaged df TEM image of the vasopressin molecule. b—The same for iodinated vasopressin. c—Model of the molecule.[91]

molecules, e.g., proteins or viruses (see Fig. 22), negative-staining methods are used.

4.2. Images of crystal structures

HREM images of crystals can be well interpreted on the basis of the existing structural (x-ray diffraction and other) data. In a number of cases they allow one to determine independently the structure and its chemical formula. Figure 28 shows an image of the crystal lattice of silicon. Here one observes individually (at the limit of resolution) Si atoms separated in projection by 1.357 Å. Figure 29a is an image of the structure of MgO, and Fig. 29b that of GaAs, in which the "atom-spots" are shifted from their actual positions owing to phase distortions.

One can attain the greatest resolution in studying simple metals using a megavolt EM (see Fig. 10), but here the fundamental defects of the method are revealed in the imaging of atoms, involving the properties of the transfer function.

Good electron micrographs are obtained now in many laboratories of the world from complex metal oxides, which are often built of MeO_6 octahedra or other polyhedra linked together by their edges (Fig. 30; see also Figs. 4 and 7). One can make the chemical formula more precise on the basis of

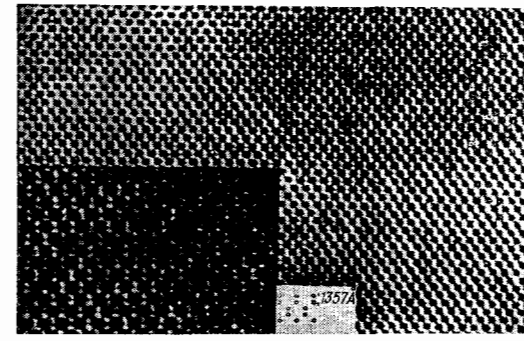

FIG. 28. Bf TEM image of the crystal structure of silicon in a projection along [110].[92] Si atoms—white spots; insets—magnified region and diagram of the structure.

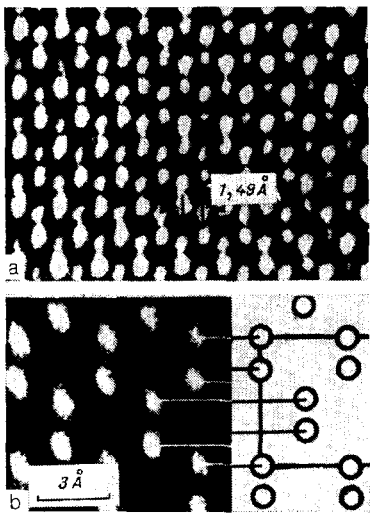

FIG. 29. a—Bf TEM image of the structure of MgO in a projection along [110] (accelerating potential 400 kV). b—Bf TEM image of atoms in the structure of GaAs and a comparison of it with the ideal positions of the atoms in the structure.[93]

such micrographs. The processing of electron micrographs can include optical or computer double Fourier transformation and allowance for the transfer function.

Structures having the general formula UW_nO_{3n+2} are built of planar blocks of varying width. Figure 31 is an electron micrograph of the structure of UW_5O_{17}. The structure consists of WO_6 octahedra forming blocks. Depending on the value of n ($n = 4, 5,$ or 6), the blocks are linked by zigzag chains of uranium atoms extended in the 100 direction. The structures with even ($n = 4, 6$) and odd n($n = 5$) are similar, but differ in that for odd n the adjacent atom chains of uranium lie "in phase," but for even n in "counterphase." The unit cell of the phase was determined from the image and the microdiffraction patterns, and the three-dimensional packing was found under the assumption that the studied structure resembles the known structure of β-UMo_2O_8 [96]

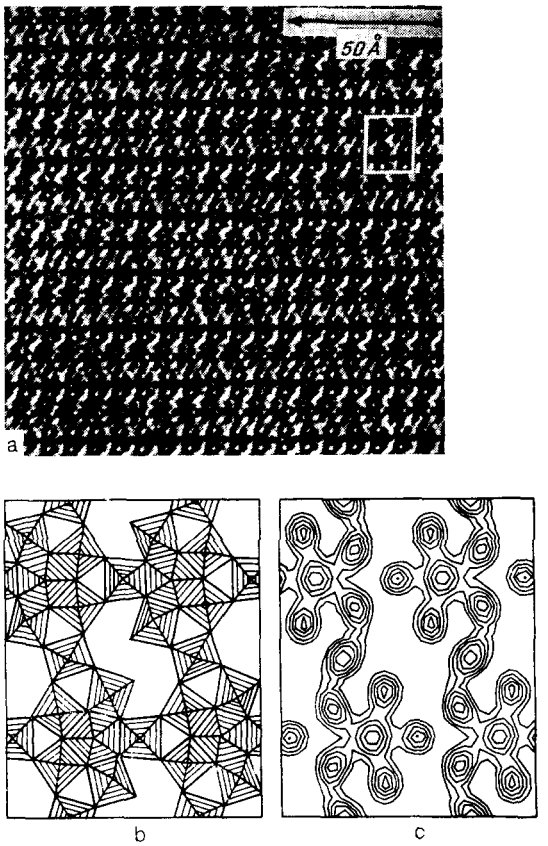

FIG. 30. a—Electron micrograph of a thin plate of the crystal structure of $K_{8-x}Nb_{16-x}W_{12+x}O_{80}$ ($x \approx 1$; magnification 4.6×10^6). b—Diagram of the structure; MeO_6 and MeO_7 polyhedra. c—Processed double Fourier transform—image of the projected potential of one unit cell of Fig. 30a as a contour plot. The peaks of the densitogram yield an image of only the W and Nb atoms blurred by the apparatus functions of the microscope. Their coordinates in the projection are determined with an accuracy of ~ 0.1 Å. JEM 200CX electron microscope, accelerating potential 200 kV.[94]

along the third [001] dimension.

An analogous example of establishing a structure from electron micrographs is the study of the crystal $2Nb_2O_5 \cdot 7WO_3$ (see Fig. 4).[5]

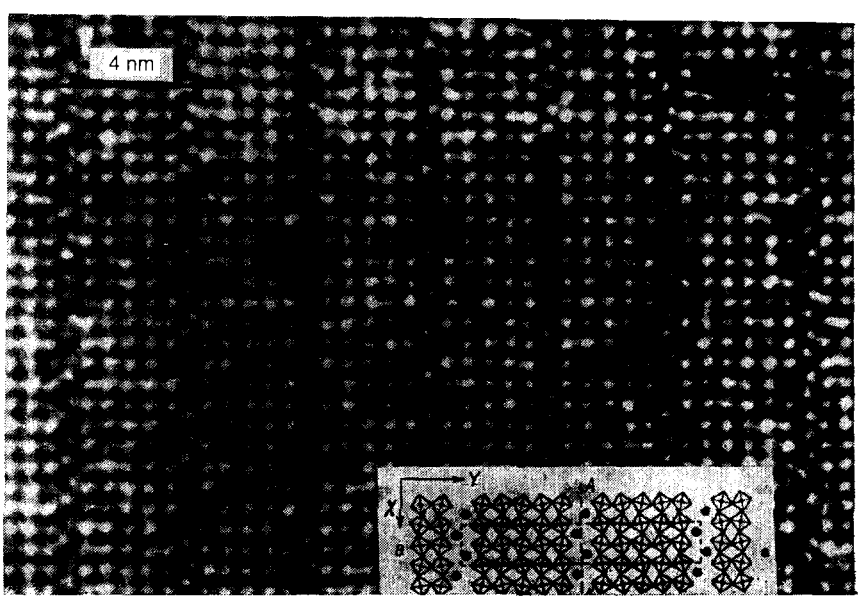

FIG. 31. Image of the crystal structure of UW_5O_{17}.[95] The arrow indicates an interlayer having the composition UW_6O_{20}. Inset—diagram of the packing of octahedra.

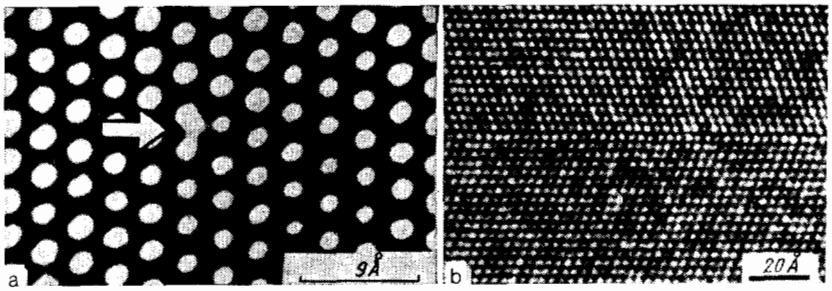

FIG. 32. Silicon lattice containing defects. a—Region containing an implanted foreign atom; resolution 3 Å; each bright spot amounts to the merged image of a pair of Si atoms (N. D. Zakharov; cf. Fig. 28). b—Twinning of the structure of Si (A. L. Vasil'ev.).

4.3. Defects in an ideal structure

The em method is unique for directly revealing the point and linear defects of a crystal structure, packing errors, and other perturbations. Point defects of the type of vacancies, inclusions, or substitutions of foreign atoms are difficult to observe, and sometimes impossible, owing to their weak contrast on the background of the relatively "thick" layer of the structure, as a column of tens of atoms is projected into each spot. Fig. 32a is the implantation of a foreign atom into a silicon lattice, and Fig. 32b shows twinning.

Implanted ions have been observed on the example of a study of the structure of Nb_2O_5.[97] The implanted ions lie in an environment of 12 O atoms and 8 Nb atoms (Fig. 33). Figure 34 shows the corresponding micrographs. One can observe well at atomic resolution the linear plane defects of packing errors in the structure of gold (Fig. 35). Figure 36a shows an observation of dislocations, and Fig. 36b the arrangement of atoms.

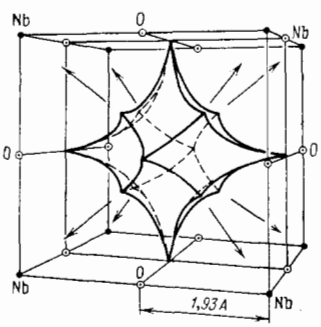

FIG. 33. Configuration of an implantation site of an ion in the Nb_2O_5 lattice.

Contemporary em technique enables one to use a television system and videorecording to record the behavior of defects in a dynamic process. Thus, specimens of CdTe have been studied during annealing in the Cambridge electron microscope (500 kV, resolution ~2 Å).[98] In the micrographs of Fig. 37 the CdTe atom pairs (columns of them lie along the axis of projection) lying at a distance of 1.6 Å are not resolved. However, the fluctuating image of the edge of the crystal was distinctly recorded, with slip and climb of dislocations.

4.4. Combined irregularly periodic structures. Nucleation of crystals

Crystallographers have long known from diffraction and other data that many structures of complex chemical composition—synthetic and natural oxides, and minerals—are constructed in such a way that they do not have an ideal three-dimensional periodicity. Electron microscopy has revealed that "blocks" can exist of strict spatial and chemical composition, but not identical, and firmly linked together, or identical blocks, but linked toegether in different ways. If the different blocks alternate regularly in space, this actually leads to the appearance of a superstructure having large periods. If they are linked irregularly, the structure has no strict periodicity. The mutual combination of identical or differing (of two, three, or four types) blocks yields a structure with a macroscopically nonstoichiometric formula, but actually this is a "compound of compounds" in a unitary crystal. HREM of this type of crystals— one can call them combined crystals—has literally opened up a new world of such structures, and has compelled us to take a new approach to the problems of formation, stability, and transitions in crystal phases. An interesting example of observing this type of phases was that started by Anderson and his associates[99] and continued further by other authors by em study of solid-state

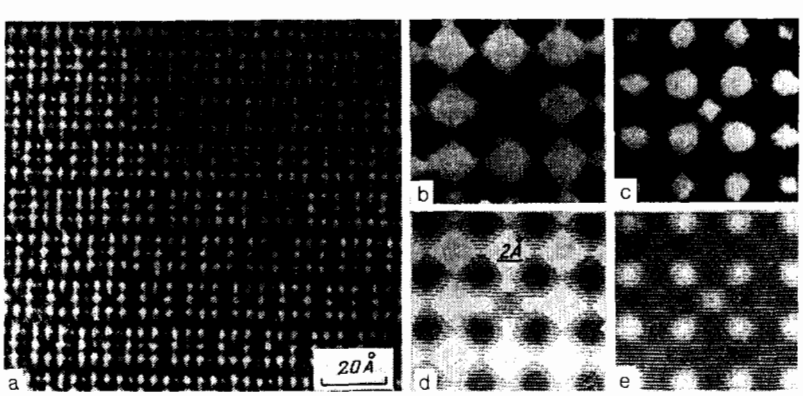

FIG. 34. Structure of niobium pentoxide. a—Em projection of the structure (defocus 300 Å). b, c—Magnified image of an implanted ion at different defocuses (– 400 and 300 Å). d, e—Calculated simulation of the images. 500-kV microscope, Kyoto.

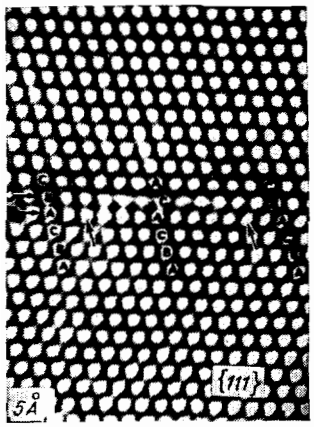

FIG. 35. Packing error of layers in the close cubic packing of gold atoms.[41]

reactions in oxides, ferrites, and other compounds.[100] Thus, in studying processes of oxidation and reduction of oxides of heavy metals of variable valency, an atomic mechanism of the crystal-structure rearrangement that occurs here was discovered and studied. The already mentioned niobium oxides based on the starting formula Nb_2O_5 form a number of structures having the gross formulas $NbO_{2.417}$, $NbO_{2.454}$, $NbO_{2.480}$, etc. As one can exactly establish from the electron micrographs, they actually correspond to the structures $Nb_{12}O_{29}$, $Nb_{22}O_{54}$, $Nb_{25}O_{62}$.... The point is that these structures are fundamentally constructed of columns of octahedra linked at their vertices and forming in cross-section $n\times m$ octahedra, e.g., 3×3, 4×3, 5×3. These columns, which are linked together by their edges, appear on electron micrographs respectively as 2×2, 3×2, and 4×2 channels, etc., as combinations of bright spots (Fig. 38).

Analogous phenomena have been found in the complex structures $Me_x WO_3$, Me = K, Rb, Cs, Te, Sn, Ba, Pb, etc.

The case is of interest in which the three-dimensional blocks (columns) are identical, but they are not linked identically, albeit regularly. A classic example is the oxides of the transition metals $Me_n O_{3n-m}$ (tungsten, molybdenum, etc.). In an ideal structure having columns of MO_6 octahedra in contact by their edges rather than vertices (Fig. 39a), a so-called "crystallographic slip" arises. Such a slip along {102} yields a structure of the $Me_n O_{3n-1}$ type, along {103} $Me_n O_{3n-2}$, etc. (Fig. 39b).

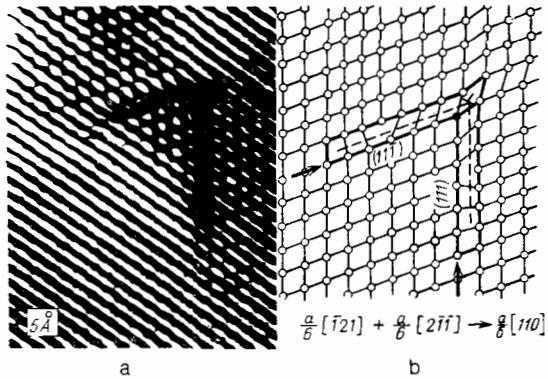

FIG. 36. Gold crystal containing two partial dislocations in different slip planes (a) and the corresponding diagram of packing of the atoms (b).[42]

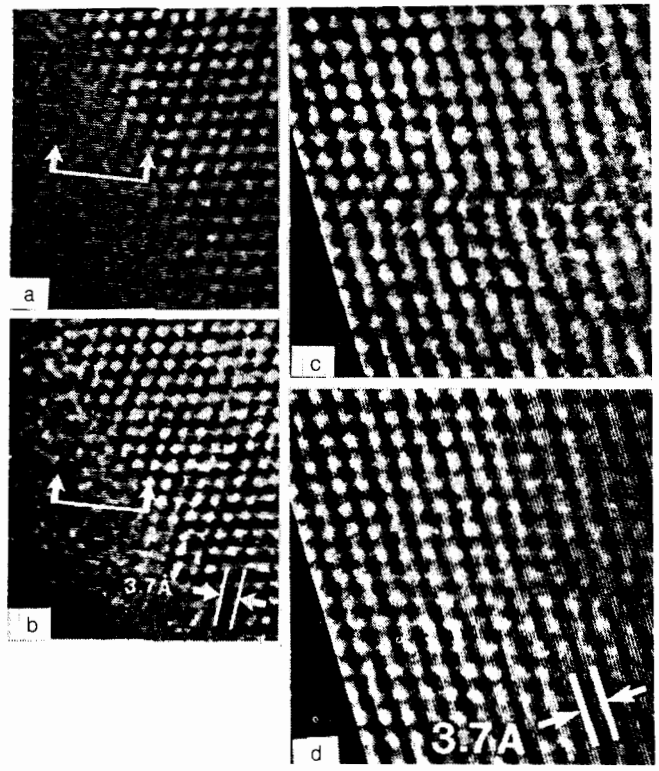

FIG. 37. Changes in the atomic structure of CdTe in the process of taking micrographs.[98] Cambridge electron microscope; 500 kV; resolution 2 Å; the observations were performed in real time with a television videosystem; white spots—pairs of CdTe atoms (cf. Fig. 32). a, b—Changes in the arrangement of atoms on an edge of the crystal; time between micrographs 0.46 s. c, d—Motion of a partial dislocation.

An alternation of two-dimensional *layers* of differing composition has been found electron-microscopically in the structure of minerals (Figs. 40, 41).

Much interesting data have been found using HREM

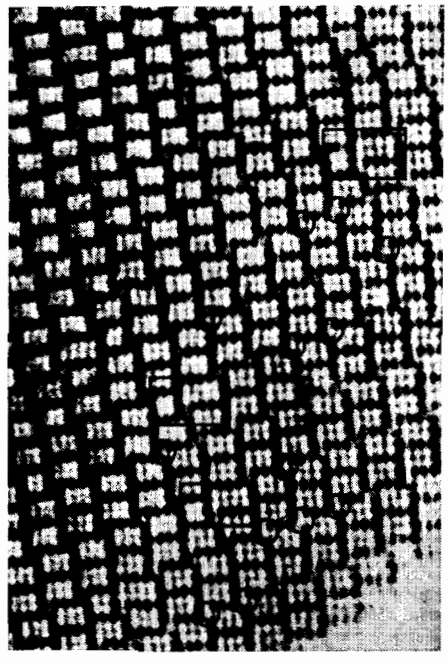

FIG. 38. Oxidized structure of $Nb_{25}O_{62}$ consisting mainly of 3×4 columns of octahedra (2×3 bright channels), but there are also 3×3 and 3×5 columns and incorrect links between the different columns.[99]

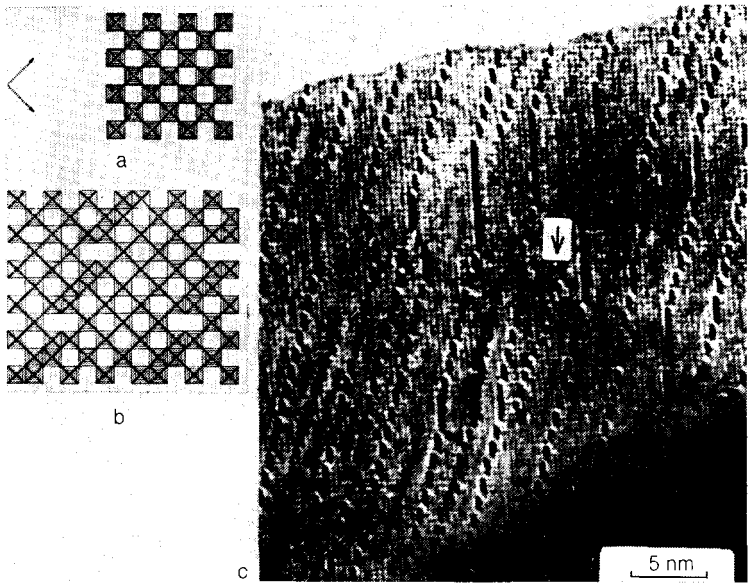

FIG. 39. "Crystallographic slip." a—Ideal structure of the WO_3 type. b—Slip along {103}. c—Structure of the composition $Ti_{0.03}WO_3$ containing mainly slip planes of the type {103}—dark lines.[100]

on the concrete arrangement of the atoms in the linking of domains or grains, and also in epitaxy, the geometry of which had previously been only suppositional. Figure 42 shows a grain boundary in NiO.[103] Figure 43 shows the structure of an intermediate layer along (100) between (Cd, Hg)Te and GaAs lattices.[104] Figure 44 shows the structure of the alloy Au_5Mn_2 after annealing, containing a large number of cubic twin boundaries.[105]

HREM enables one to observe directly epitaxy processes on the atomic level of resolution. This is currently especially important in studying processes of formation of semiconductor heterostructures employed in microelectronics. Figure 45 shows the epitaxial growth of Si on sapphire (Al_2O_3). Fig. 46 shows a multilayer heterostructure GaAs/AlAs.[107]

It is of great interest to study nucleation of crystals, and in particular, microcrystalline concretions[108,109] (Fig. 47). New data have been obtained on the structure of crystal surfaces. It turns out that the classical view in crystallography of the uniform filling by atoms of rational faces, as is shown in Fig. 48, is not always realized (Fig. 49).

A recent study was not only able to establish[111] that intense migration occurs in the growth of gold crystals—"hopping" of atoms on the surface (cf. Fig. 37), but also observed that the crystal is surrounded by a "cloud" of atoms that continually exchange with the atoms of the surface of the crystal (Fig. 50). The "clouds" of gold atoms extend to a distance up to 8–9 Å from the surface and continually change in shape and density. This was observed in recording the em patterns at atomic resolution on a television videorecorder in real time.

5. CONCLUSION

We have examined the theoretical aspects of high-resolution electron microscopy and the experimental data on the structure of matter, mainly crystals, at the atomic level, as obtained by HREM.

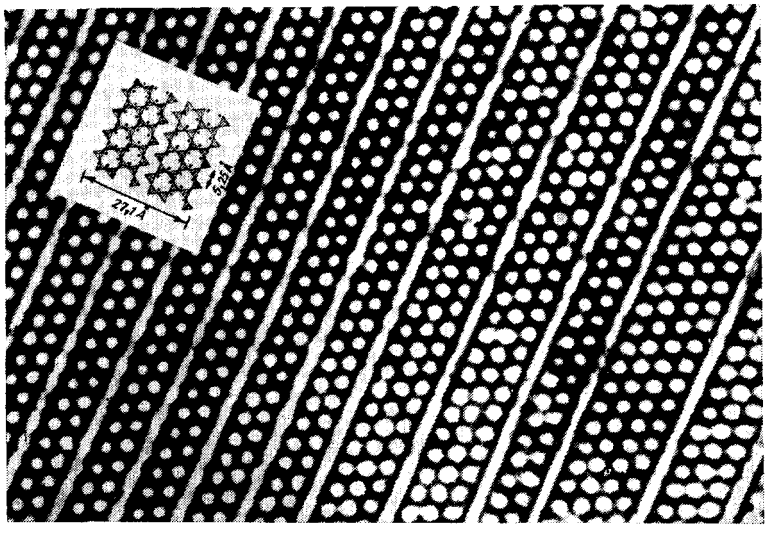

FIG. 40. Na-Co-silicate.[101] Inset—diagram of the structure; triangles—projections of SiO_4 tetrahedra, dots—metal atoms lying in octahedral environments made of oxygen atoms. The light interstices in the photograph and the diagram are the "windows" in the structure. One can see ternary (with two rows of holes), quaternary (with three rows), and quinary (with four rows) chains of octahedra.

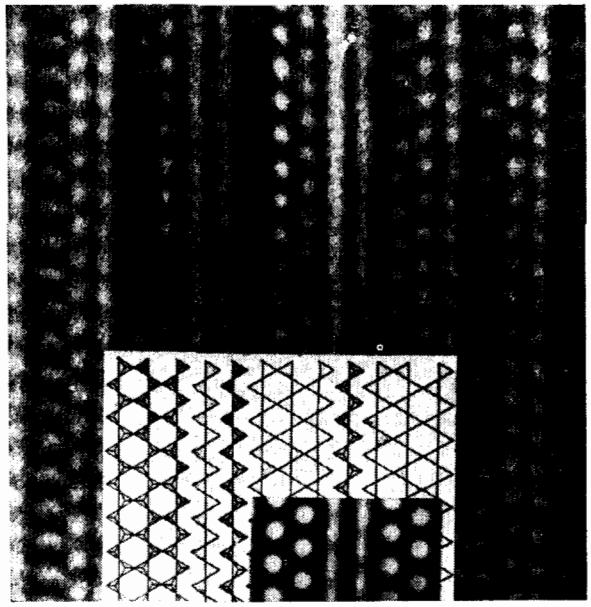

FIG. 41. Na-Co-silicate.[102] The insets show a diagram of the structure and the calculated image of the pyroxene chain.

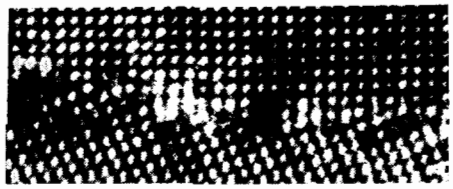

FIG. 42. Grain boundary in NiO.[103]

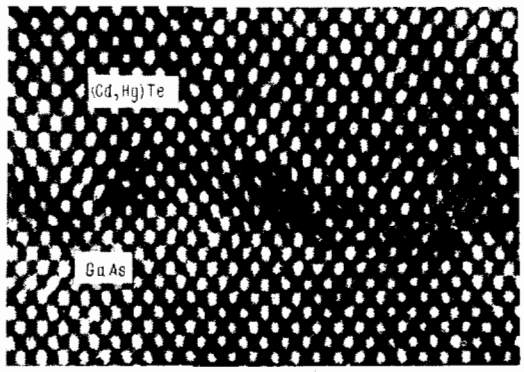

FIG. 43. Arrangement of atoms in an intermediate layer between (Cd, Hg) Te and GaAs.[104] The lattice mismatch (15%) is compensated by a series of dislocations.

The theoretical estimates of resolution, contrast, and character of the electron scattering agree well with experiment, but individual unclear problems still remain in the theory. The accuracy of EM with respect to the geometry of arrangement of atoms and the intensity of peaks representing atoms is relatively low.

Wherein lies the attractiveness of this method? Indeed, a vast amount of experimental data obained by other methods is available on the existence of atoms, their dimensions, and their arrangement in molecules and crystals. However, all these data result from rather complicated and often indi-

FIG. 44. A "carpet" of domains in the alloy Au_5Mn_2 after annealing.[105] The domain boundaries often amount to twinning of the adjacent cubic packings.

FIG. 45. Electron micrograph of the phase boundary of an epitaxial Si film on an Al_2O_3 substrate.[106] The Si region lies in the standard epitaxial relationship with the substrate.

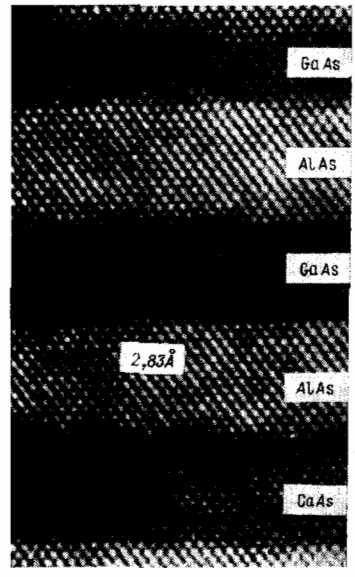

FIG. 46. Electron micrograph of a multilayer superlattice of GaAs/AlAs heterolayers along [110]. Owing to the similarity of the lattice parameters, the layers of differing composition congruently pass into one another.[107]

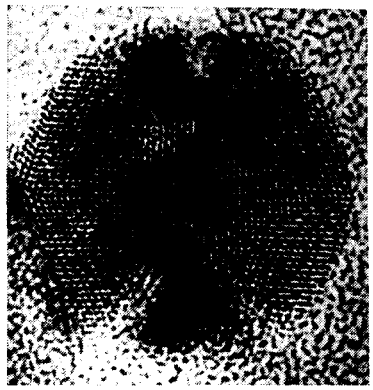

FIG. 47. Submicroscopic icosahedral junction of microcrystals of silver.[108]

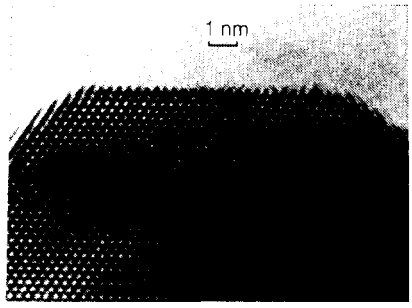

FIG. 48. Classical atomically smooth structure of a (100) face of a ZrO_2 crystal. The Zr atoms lie with a spacing of 0.36 nm.[110]

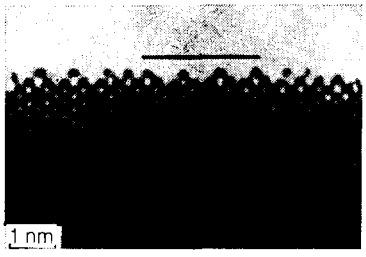

FIG. 49. Region of a (110) face of gold having a surface 2×1 superstructure.[108]

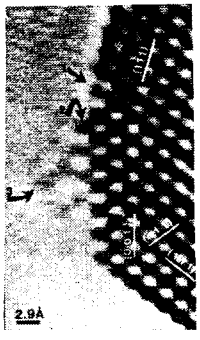

FIG. 50. Image of the (001) profile of an Au crystal along the direction [110]. Arrows: *1*—$(1\bar{1}1)$ twinning plane, *2*—column of seven Au atoms (along the direction of projection), *3*—"cloud" of Au atoms. Time of recording 0.31 s (raster of the image is the scan on the monitor).[111]

rect measurements from which one can construct the structure of the object of interest to us. However, the human mind values most of all the direct perception of the facts regarding the object of study. In this sense electron microscopy brings the atomic structure of matter closest to the investigator, and directly yields the picture in which we are interested. The point is also important that one can do this quickly. Of course, also here an attentive analysis and refining processing of the experimental results are needed. Processing and calculation of images on line with a computer open up great potentialities.

While the EM is considerably inferior to the diffraction methods in regard to obtaining data on the structure of "ideal," three-dimensionally periodic crystals and individual molecules, it is in no way replaceable in studying the real structure of crystals with various variations and perturbations of the ideal structure. The possibility of observing the dynamics of atomic structure is especially valuable—migrations of atoms and defects on a real time scale using television monitors.

The limitations of electron microscopy are the special requirements on the specimens and their preparation, and the difficulty of studying materials consisting of light atoms. The electron microscope is a very complicated instrument, but of course, further refinement of its design will take place, especially with the aim of obtaining even higher resolution. Without any doubt, electron microscopy will develop even further, and will offer much valuable data for solid-state physics and chemistry, crystallography, mineralogy, biology, in studying high-technology materials, in studying and monitoring various devices of micro-, and subsequently, of molecular electronics.

The 11th International Congress on Electron Microscopy occurred from August 31 to September 7, 1986 in Kyoto.[112] Very many studies were presented there on the "nanoworld," i.e., studies on electron microscopy at atomic resolution. Studies have been intensively developed on various semiconductor structures, including superstructures and heterostructures, on the surfaces of crystals during growth and epitaxy, and on the surfaces of superstructures. Special transmission electron microscopes at elevated voltages have been developed for such studies (e.g., the JEM-2000 FXV), with a vacuum down to 10^{-9} Torr. Electron micrographs taken with image intensifiers made a great impression. In this "atomic cinema" in real time, processes were recorded of migration of atoms and rearrangement of the atomic structure of a surface, transformation of the atomic structure of gold clusters on the surface of a carbon film, etc. Electron micrographs were demonstrated of the structure of "quasicrystals," [113] the atomic packing in which is characterized by fivefold icosahedral symmetry. Scanning electron microscopes have been built with a guaranteed resolution better than 15 Å.

A remarkable event of 1986 was the award to the inventor of the electron microscope Ernst Ruska,[1,2] of the Nobel Prize in physics, which stressed the vast importance of this method in modern physics and technology.

[1)]We shall employ the abbreviations: EM—electron microscopy; em—electron-microscopic; as well as the abbreviations generally adopted in the current literature: TEM—transmission electron microscopy; STEM—scanning transmission electron microscopy; HREM—high-re-

solution electron microscopy; the latter is electron microscopy at atomic resolution.

[2)]In electron microscopy one can neglect the change in the outer electron shells, and correspondingly in the potential, in forming chemical bonds between the atoms in crystals and molecules.

[3)]The author has described this and certain other methods of processing electron micrographs in a review in Usp. Fiz. Nauk in 1973.[74]

[1]M. Knoll and E. Ruska, Ann. Phys. (Leipzig) **12**, 607, 641 (1932).
[2]E. Ruska, *The Early Development of Electron Lenses and Electron Microscopy*, S. Hirzel Verlag, Stuttgart, 1980.
[3]J. W. Menter, Proc. R. Soc. London Ser. A **236**, 119 (1956).
[4]H. Hashimoto, A. Kumao, K. Hino, H. Yotsumoto, and A. Ono, Jpn. J. Appl. Phys. **10**, 1115 (1971).
[5]J. M. Cowley and S. Iijima, *The Electron Microscope in Mineralogy*, Springer-Verlag, Berlin, 1976.
[6]O. Scherzer, J. Appl. Phys. **20**, 20 (1949).
[7]C. B. Eisenhander and B. M. Siegel, *ibid.* **37**, 1613 (1966).
[8]W. Hoppe, Chem. Scripta **14**, 227 (1978–1979).
[9]J. M. Cowley, Ann. Rev. Mat. Sci. **6**, 53 (1976).
[10]J. M. Cowley, Ultramicrosc. **8**, 1 (1982).
[11]J. M. Cowley, *Diffraction Physics*, North-Holland, Amsterdam, 1975.
[12]K.-J. Hanszen, Z. angew. Phys. **27**, 125 (1969).
[13]A. A. Vyazigin, Izv. Akad. Nauk. SSSR Ser. Fiz. **36**, 1917 (1972) [Bull. Acad. Sci. USSR Phys. Ser. **36**, 1694 (1972)].
[14]F. Thon, 8th Intern. Congress of Electron Microscopy, Canberra, 1974, Vol. 1, p. 238.
[15]E. J. Kirkland, B. M. Siegel, N. Uyeda, and Y. Fujiyoshi, Ultramicrosc. **5**, 479 (1980).
[16]E. J. Kirkland, B.M. Siegel, N. Uyeda, and Y. Fujiyoshi, *ibid.* **17**, 87 (1985).
[17]B. K. Vaĭnshteĭn, Structural Electron Diffraction (in Russian), Izd-vo AN SSSR, M., 1956.
[18]W. K. Pratt, *Digital Image Processing*, Wiley, New York, 1978 [Russ. transl., Mir, M., 1982].
[19]R. O. Duda and P. E. Hart, *Pattern Classification and Scene Analysis*, Wiley, New York, 1973 (Russ. transl., Mir, M., 1976).
[20]P. W. Hawkes, ed., *Computer Processing of Electron Microscope Images*, Springer-Verlag, Berlin, 1980.
[21]G. Thomas and M. J. Goringe, *Transmission Electron Microscopy of Materials*, Wiley, New York, 1979 [Russ. transl., Nauka, M., 1983].
[22]J. C. H. Spence, *Experimental High-Resolution Electron Microscopy*, Clarendon Press, Oxford, 1981.
[23]G. S. Gritsaenko, B. B. Zvyagin, R. V. Boyarskaya *et al.*, Methods of Electron Microscopy of Minerals (in Russian), Nauka, M., 1969.
[24]*Advances in Optical and Electron Microscopy*, Vol. 7, Academic Press, London, 1978.
[25]I. G. Stoyanova and I. F. Anaskin, Foundations of the Methods of Transmission Electron Microscopy (in Russian), Nauka, M., 1972.
[26]V. A. Drits, Structural Study of Minerals by Methods of Microdiffraction and High-Resolution Electron Microscopy (in Russian), Nauka, M., 1972.
[27]P. B. Hirsch, A. Howie, R. B. Nicholson, D. W. Pashley, and M. J. Whelan, *Electron Microscopy of the Thin Crystals*, Butterworths, London, 1965 [Russ. transl., Mir, M., 1968].
[28]H.-R. Wenk, ed., *Electron Microscopy in Mineralogy*, Springer-Verlag, Berlin, 1976 [Russ. transl., Mir, M., 1979].
[29]M. Born, Z. Phys. **37**, 863 (1926); **38**, 803 (1926).
[30]H. A. Bethe, Ann. Phys. (Leipzig) **87**, 55 (1928).
[31]M. Blackman, Proc. R. Soc. London Ser. A **173**, 68 (1939).
[32]Z. G. Pinsker, Electron Diffraction (in Russian), Izd-vo AN SSSR, M.-L., 1949.
[33]M. Born and E. Wolf, *Principles of Optics*, 4th, ed., Pergamon Press, Oxford (1970) [Russ. transl., Nauka, M., 1973].
[34]S. Horinchi, Chem. Scripta **14**, 75 (1978–1979).
[35]J. M. Cowley and A. F. Moodie, Proc. R. Soc. London Ser. A **76**, 3378 (1960).
[36]G. R. Grinton and J. M. Cowley, Optik **34**, 221 (1971).
[37]M. V. Berry and K. E. Mount, Rep. Prog. Phys. **35**, 315 (1972).
[38]P. A. Doyle, Acta Crystallogr. Sect. A **26**, 569 (1969).
[39]A. A. Vyazigin and Yu. B. Vorob'ev, Izv. Akad. Nauk SSSR, Ser. Fiz. **27**, 1122 (1963) [Bull. Acad. Sci. USSR Phys. Ser. **27**, 1103 (1963)].
[40]H. Hashimoto, E. Endoh, Y. Takai, H. Tomioka, and Y. Yokota, Chem. Scripta **14**, 23 (1978–1979).
[41]W. Hoppe, Philos. Trans. R. Soc. London Ser. B **261**, 71 (1971).
[42]H. Hashimoto, Y. Yokota, Y. Takai, H. Endoh, and A. Kumao, Chem. Scripta **14**, 125 (1978–1979).
[43]A. A. Danishevskiĭ and F. N. Chukovskiĭ, Kristallografiya **27**, 668 (1982) [Sov. Phys. Crystallogr. **27**, 401 (1982)].
[44]K. J. Hanszen, Microscopie Electronique, Grenoble, 1970, ed. P. Favard, Société Française de Microscopie Électronique, Paris, 1970, Vol. 1, p. 45.
[45]J. G. Allpress, E. A. Hewat, A. F. Moodie, and J. V. Sanders, Acta Crystallogr. Sect. A **28**, 528 (1972).
[46]B. Jouffrey, D. Dorignac, and M. Tanaka, Chem. Scripta **14**, 63 (1978–1979).
[47]J. M. Cowley, Acta Crystallogr. Sect. A **29**, 529 (1973).
[48]N. D. Zakharov, V. N. Rozhanskiĭ, and E. V. Parvova, Fiz. Tverd. Tela (Leningrad) **22**, 3208 (1980) [Sov. Phys. Solid State **22**, 1877 (1980)].
[49]A. V. Crewe, J. Electron Microsc. **28**, S-9 (1979).
[50]A. V. Crewe, Chem. Scripta **14**, 17 (1978–1979).
[51]A. V. Crewe, J. P. Langmore, and M. S. Isaacson, *Physical Aspects of Electron Microscopy and Microbeam Analysis*, Wiley, New York, 1975, p. 47.
[52]J. M. Cowley, M. A. Osman, and P. Humble, Ultramicrosc. **15**, 311 (1984).
[53]R. W. Carpenter and J. C. H. Spence, J. Microsc. **136**, 165 (1984).
[54]B. K. Vaĭnshteĭn, Tr. IK AN SSSR, No. 11, 78 (1955).
[55]B. K. Vaĭnshteĭn and V. F. Dvoryankin, Kristallografiya **1**, 626 (1956) [Sov. Phys. Crystallogr. **1**, 493 (1956)].
[56]R. Glauber and V. Schomaker, Phys. Rev. **89**, 667 (1953).
[57]B. K. Vaĭnshteĭn, Veröffentlichungen zur 10. Tagung "Elektronenmikroskopie," Leipzig, 1981, Vol. 1, p. 11.
[58]Z. G. Pinsker, X-Ray Crystal Optics (in Russian), Nauka, M., 1982.
[59]R. D. Heidenreich, *Fundamentals of Transmission Electron Microscopy*, Interscience, New York, 1964 [Russ. transl., Mir, M., 1966].
[60]K. Jujiwara, J. Phys. Soc. Jpn. **14**, 1513 (1959).
[61]F. Fujimoto and A. Howie, Philos. Mag. **13**, 1131 (1966).
[62]P. Goodman and A. F. Moodie, Acta Crystallogr. Sect. A **30**, 280 (1974).
[63]H. Niehrs, Z. Naturforsch. **149**, 504 (1959).
[64]L. Sturkey, Proc. Phys. Soc. London **80**, 321 (1962).
[65]L. T. Chadderton, in: *Channeling: Theory, Observation and Application*, ed. D. V. Morgan, Wiley, London, 1973.
[66]H. Hashimoto, A. Howie, and M. J. Whelan, Proc. R. Soc. London Ser. A **269**, 80 (1962).
[67]N. Kato, J. Phys. Soc. Jpn. **7**, 397 (1952).
[68]K. Kambe, Ultramicrosc. **10**, 223 (1982).
[69]H. Hashimoto, M. Mannami, and T. Naiki, Philos. Trans. R. Soc. London **253**, 459, 490 (1961).
[70]C. G. Darwin, Philos. Mag. **27**, 315, 675 (1914).
[71]J. M. Cowley and A. F. Moodie, Acta Crystallogr. **10**, 609 (1957).
[72]H. P. Erickson and A. Klug, Philos. Trans. R. Soc. London Ser. B **261**, 105 (1971).
[73]V. P. Kosykh, A.I. Puskovskikh, V. S. Kirichuk, T. Kyune, E. V. Orlova, V. P. Tsuprun, and N. A. Kiselev, Kristallografiya **28**, 1082 (1983) [Sov. Phys. Crystallogr. **28**, 637 (1983)].
[74]B. K. Vaĭnshteĭn, Usp. Fiz. Nauk **109**, 455 (1973) [Sov. Phys. Usp. **16**, 185 (1973)].
[75]N. A. Kiselev, Modern Electron Microscopy in the Study of Matter (in Russian), Nauka, M., 1982, p. 167.
[76]M. B. Sherman, E. V. Orlova, S. S. Terzyan, R. Kleine, and N. A. Kiselev, Ultramicrosc. **7**, 131 (1981).
[77]R. A. Crowther and L. A. Amos. J. Mol. Biol. **60**, 123 (1971).
[78]J. Frank, see Ref. 20, p. 187.
[79]M. Skeinkilberg and H. J. Schramm, Z. Physiol. Chem. **361**, 1363 (1980).
[80]M. Van Hill, Ultramicrosc. **13**, 165 (1984).
[81]N. Uyeda, T. Kobayashi, K. Ishizuka, and Y. Fujiyoshi, Chem. Scripta **14**, 17 (1978–1979).
[82]A. Klug and D. J. de Rosier, Nature **212**, 29 (1966).
[83]P. L. Fejes, S. Iijima, and J. M. Cowley, Acta Crystallogr. Sect. A **29**, 710 (1973).
[84]A. L. Vasiliev, O. V. Uvarov, M. A. Gribeluk, N. A. Kiselev *et al.*, Proc. 11th Internat. Congr. of Electron Microscopy, Kyoto, Japan, Aug. 31–Sep. 7, 1986, p. 1391.
[85]M. Beer, J. W. Wiggins, D. Tunkel, and C. K. Stoechert, Chem. Scripta **14**, 263 (1978–1979).
[86]E. J. Kirkland, Ultramicrosc. **15**, 151 (1984).
[87]B. K. Vaĭnshteĭn, Modern Crystallography, Vol. 1 (in Russian), Nauka, M., 1979.
[88]Yu. Z. Nozik, R. P. Ozerov, and K. Khennig, Structural Neutron Diffraction, Vol. 1 (in Russian), Atomizdat, M., 1979.
[89]M. F. C. Ladd and R. A. Palmer, eds., Theory and Practice of Direct Methods in Crystallography, Plenum Press, New York, 1980 [Russ. transl., ed. B. K. Vaĭnshteĭn, Mir, M., 1983].
[90]P. N. T. Unwin and R. Henderson, J. Mol. Biol. **94**, 425 (1975).
[91]F. R. Ottensmeyer, D. P. Bazett-Jones, R. M. Henkelman, A. P. Korn, and R. F. Whiting, Chem. Scripta **14**, 257 (1978–1979).
[92]K. Izui, S. Furuno, T. Nishida, and H. Otsu, *ibid.*, p. 99.
[93]H. Hashimoto, Ultramicrosc. **18**, 19 (1985).
[94]S. Hovmöller, A. Sjögren, G. Farrants, M. Sundberg, and B. O. Marinder, Nature **311**, 238 (1984).
[95]N. D. Zakharov, M. A. Gribeluk, B. K. Vaĭnshteĭn, O. N. Rozanova, K.

Uchida, and S. Horinchi, Acta Crystallogr. Sect. B **39**, 575 (1983).
[96]L. M. Kovba, O. N. Rozanova, and V. K. Trunov, Radiokhimiya **19**, 260 (1977).
[97]N. Uyeda, Y. Fujiyoshi, and K. Ishizuka, Ultramicrosc. **15**, 139 (1984).
[98]R. Sinclair, F. A. Ponce, T. Yamashita, D. J. Smith, R. A. Camps, L. A. Freeman, S. J. Erasmus, W. C. Nixon, K. C. A. Smith, and C. J. D. Catto, Nature **298**, 127 (1982).
[99]J. S. Anderson, Chem. Scripta **14**, 129 (1978–1979).
[100]R. J. D. Tilley, *ibid.*, p. 147.
[101]V. A. Drits, N. D. Zakharov, and I. P. Khadzhi, Izv. Akad. Nauk SSSR Ser. Geol., No. 11, 82 (1979).
[102]N. D. Zakharov, I. P. Khadzhi, and V. N. Rozhanskiĭ, Dokl. Akad. Nauk SSSR **249**, 359 (1979) [Sov. Phys. Dokl. **24**, 877 (1979)].
[103]K. L. Merkle, J. F. Reddy, and C. L. Wiley, Ultramicrosc. **18**, 281 (1985).
[104]J. L. Hutchinson, *ibid.*, p. 349.
[105]S. Amelinckx, Chem. Scripta **14**, 197 (1978–1979).
[106]A. L. Vasil'ev, A. L. Golovin, K. M. Manafov, R. M. Imamov, and N. A. Kiselev, Poverkhnost', p. 123 (1987).
[107]M. P. A. Vieqers, A. F. De Yong, and M. R. Leys, Spectrochem. Acta Ser. B **40**, 835 (1985).
[108]D. Y. Smith and L. D. Marks, Ultramicrosc. **16**, 101 (1985).
[109]L. D. Marks, *ibid.* **18**, 445 (1985).
[110]C. E. Warble, *ibid.* **15**, 301 (1984).
[111]J. O. Bovin, R. Wallenberg, and D. J. Smith, Nature **317**, 47 (1985).
[112]Electron Microscopy 1986: Proc. 11th Internat. Congress on Electron Microscopy, Kyoto, Aug. 31–Sep. 7, 1986, Vol. 1, 2: Suppl. to J. Electron Microsc. **35** (1986).
[113]D. S. Shechtman, L. Blech, D. Gratias, and J. W. Cahn, Phys. Rev. Lett. **53**, 1951 (1984).

Translated by M. V. King